

## Characterization of supramolecular gels

Guocan Yu, Xuzhou Yan, Chengyou Han and Feihe Huang\*

Cite this: *Chem. Soc. Rev.*, 2013, **42**, 6697

Received 28th February 2013

DOI: 10.1039/c3cs60080g

[www.rsc.org/csr](http://www.rsc.org/csr)

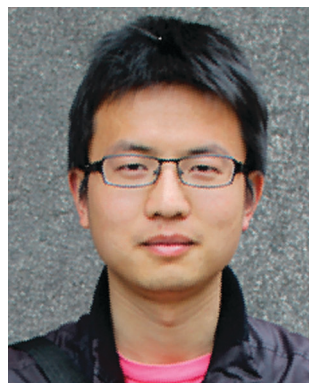
Supramolecular gels are a fascinating class of soft materials. Their gelators can self-assemble into nano- or micro-scale superstructures, such as fibers, ribbons, sheets and spheres in an appropriate solvent, thereby resulting in the formation of 3D networks. The dynamic and reversible nature of the non-covalent interactions that contribute to the formation of these network structures together gives these supramolecular gels the inherent ability to respond to external stimuli. However, the dynamic nature of supramolecular gels, which endows them with unique properties, makes their characterization diversified at the same time. Therefore, we present here a review summarizing various methods for characterizing supramolecular gels, including nuclear magnetic resonance spectroscopy, computational techniques, X-ray techniques, microscopy techniques, dynamic light scattering, thermal analysis, and rheology. Based on the gelation mechanisms and influencing factors of supramolecular gels, suitable and sufficient characterization methods should be carefully employed to make full use of their respective advantages to better investigate these materials.

### 1. Introduction

Soft materials have been attracting increasing attention as a “transformable” functional class of materials, owing to their moderate mobility and flexibility, which readily enables them to change their bulk shape and properties depending on the conditions.<sup>1</sup> Gels are soft materials that are reasonably less

mobile agglomerates with mechanical properties ranging from soft and weak to hard and tough.<sup>2</sup> Gels are defined as substantially dilute cross-linked systems, which exhibit no flow in the steady-state.<sup>3</sup> This internal network structure may result from physical bonds (physical gels) or chemical bonds (chemical gels), as well as crystallites or other junctions that remain intact within the extending fluid.<sup>4</sup> Virtually any fluid can be used as an extender including water (hydrogels, edible jelly is a common example of a hydrogel and has approximately the density of water), an organic solvent (organogels), and even

Department of Chemistry, Zhejiang University, Hangzhou 310027, P. R. China.  
E-mail: [fhuang@zju.edu.cn](mailto:fhuang@zju.edu.cn); Fax: +86-571-8795-3189; Tel: +86-571-8795-3189



Guocan Yu

Guocan Yu was born in Zhejiang, China in 1987. He received his BS degree in polymer materials and engineering from Hefei University of Technology in 2010. Then he joined the laboratory of Prof. Feihe Huang at Zhejiang University to pursue his PhD degree in chemistry. His current research interests are focused on controllable self-assembly based on pillararenes and their biologically relevant applications.



Xuzhou Yan

Xuzhou Yan was born in Jiangsu, China in 1986. He received his BS degree in chemistry from Zhejiang Sci-Tech University under the supervision of Prof. Xuming Zheng in 2009. Then he joined the laboratory of Prof. Feihe Huang at Zhejiang University to pursue his PhD degree in chemistry. From October 2012 to April 2013, he worked as an exchange PhD student in the laboratory of Prof. Peter J. Stang at University of Utah. His current research interests are focused on controllable self-assembly based on crown ether derivatives, supramolecular polymer materials, and coordination-driven supramolecular assemblies.

air (aerogels).<sup>5</sup> Gels have solid-like rheology and do not flow, despite being predominantly liquid in composition, typically 99% by weight of the gel while the remaining 1% is the gelator. It is the crosslinks within the fluid that give a gel its structure (hardness) and contribute to stickiness (tack). In other words, a gel is a dispersion of a gelator in a suitable fluid in which the fluid is the continuous phase while the solid is the discontinuous phase.<sup>6</sup>

Gels can be classified in different ways depending on their origins, constitutions, the types of cross-linking that creates their 3D networks and the media they encompass. In 1974, Flory classified gels into four main kinds: (1) well ordered lamellar structures, including gel mesophases, (2) disordered covalent polymeric networks (*e.g.*, vulcanized rubber and phenolic resins), (3) polymer networks formed through physical aggregation (*e.g.*, gelatin), and (4) particulate, disordered structures (*e.g.*, precipitates consisting of highly anisotropic particles or reticular networks of fibers).<sup>7</sup>

Most of the gels incorporate solvent molecules into a 3D entangled network of dimensionally controlled fibrils and tape-like organized aggregates consisting of gelators; thus far, the syntheses of functional gels and the examination of their physical properties have been focused mainly on those obtained from polymer gelators.<sup>8</sup> Supramolecular gels often consist of low-molecular weight gelators (LMWGs) that can self-assemble in an appropriate solvent into nano- or micro-scale network structures, such as fibers, ribbons, sheets and spheres, resulting in the formation of 3D networks,<sup>9–22</sup> which are interconnected by multiple non-covalent interactions, such as hydrogen bonding, metal coordination, van der Waals interactions,  $\pi$ - $\pi$  stacking interactions, solvophobic forces (hydrophobic forces for hydrogels), *etc.*<sup>23–26</sup> (Fig. 1)

Conventional polymer networks interconnected by covalent bonds cannot be redissolved and are thermally irreversible.<sup>27</sup>

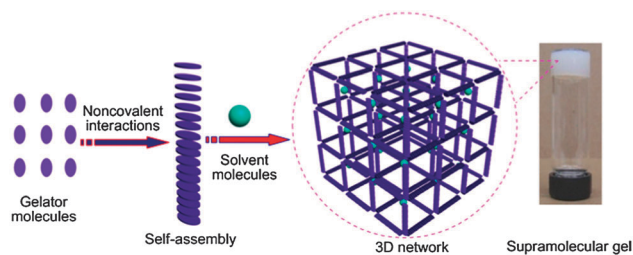


Fig. 1 Schematic representation of the formation of a supramolecular gel.

However, the dynamic and reversible nature of the non-covalent interactions that hold their network structures together results in the inherent ability of supramolecular gels to respond to external stimuli, such as temperature, pH, solvent, light, and redox reactions.<sup>28–31</sup> The stimuli-responsiveness of these novel soft materials makes them very important in materials science. For example, some supramolecular gels are sensitive to light or chemical entities by incorporating a spectroscopically active group or a receptor unit as part of the gelator. This makes them applicable in many fields, such as sensing and actuating. The diversity of the gel microstructures has allowed them to be utilized as templates to prepare novel inorganic superstructures for possible applications in catalysis and separation. Gels derived from liquid crystals (anisotropic gels) that can act as dynamically functional materials (for example, re-writable information recording) have been prepared. Supramolecular gels can also serve as media for a range of applications, such as biomaterials, sensors, liquid crystalline materials, electronic materials, and personal care formulations.<sup>32–35</sup>

However, the dynamic nature of noncovalent interactions that connect the gelator molecules for the formation of supramolecular gels also brings great difficulties to characterize supramolecular gels. In order to fully investigate these soft



Chengyou Han

Chengyou Han received his BS degree in chemistry from Zhejiang University in 2008. Then he joined the laboratory of Prof. Feihe Huang at Zhejiang University to pursue his PhD in chemistry. His current research interests are focused on host-guest chemistry based on pillararenes and supramolecular polymers.



Feihe Huang

Feihe Huang was born in China in 1973. He obtained his degree of Doctor of Philosophy in Chemistry from Virginia Polytechnic Institute and State University (VT) under the guidance of Prof. Harry W. Gibson in March 2005. Then he joined Prof. Peter J. Stang's group at University of Utah as a postdoctoral researcher. He became a Professor of Chemistry at Zhejiang University in December 2005. His current research interests are supramolecular polymers and pillararene supramolecular chemistry. The awards he received up to now include the 2004 Chinese Government Award for Outstanding Self-Financed Students Abroad, the Outstanding PhD Dissertation Award from VT, the Thieme Chemistry Journals Award, and Humboldt Fellowship for Experienced Researchers.

materials, we must be clear about the advantages and disadvantages of each characterization method and how different characterization methods can be chosen and combined based on the gelation mechanism and influencing factors of each supramolecular gel. Herein, we discuss various characterization methods and their application in investigating supramolecular gels.

## 2. Nuclear magnetic resonance (NMR) spectroscopy

Nuclear magnetic resonance (NMR) spectroscopic investigation of supramolecular gels arises from its unique ability to probe the environment of an individual atomic nucleus, reporting on the structures and dynamics of the formed networks. NMR spectra can provide information about the structural properties of the components, the resulting aggregates and the regions participating in the interactions, which play crucial roles in the stability of the dynamic networks. On the other hand, the relatively long relaxation times of the observed nuclei make NMR a powerful technique in the characterization of supramolecular gels. This is tantamount to a long memory, allowing nuclei to integrate information about different environments visited through chemical interactions or molecular motions. Thus NMR is a powerful technique for studying supramolecular gels on the molecular scale and it is suitable to provide a dynamic picture of supramolecular gels.<sup>36–41</sup>

### 2.1 <sup>1</sup>H NMR spectroscopy

<sup>1</sup>H NMR probes hydrogen nuclei within the molecules of a substance in order to determine the structure and the interactions of its molecules. Chemical shift changes can be monitored, accompanied by the formation of supramolecular gels which are driven by noncovalent interactions.

Fang and co-workers designed four novel cholesterol-appended ferrocene derivatives linked by different diamino units.<sup>42</sup> Gelation abilities of these four compounds changed dramatically due to the different lengths of the linkers. Compound **1** showed excellent gelation ability; it forms supramolecular gels in almost all solvents. Notably, the critical gelation concentration (CGC) in cyclohexane is only 0.09% by weight, which can be subsumed into the category of “super-gelators”.<sup>43</sup> Compound **2** with a longer linker, however, required distinctly higher concentration (2.5%, w/v) and longer time to gelate cyclohexane. However, for compounds **3** and **4**, gelating abilities were completely lost. Concentration- and temperature-dependent <sup>1</sup>H NMR studies were conducted to investigate the interactions between the gelators. The two signals corresponding to the two N–H groups gradually shifted downfield with increasing the concentration of **1** (Fig. 2c), indicating the formation of hydrogen bonds. On the contrary, with the increase of the solution temperature, the two signals shifted gradually upfield, suggesting breakage of the hydrogen bonds (Fig. 2d).

Huang and coworkers recently demonstrated a multiresponsive, shape-persistent, and elastic supramolecular polymer network gel

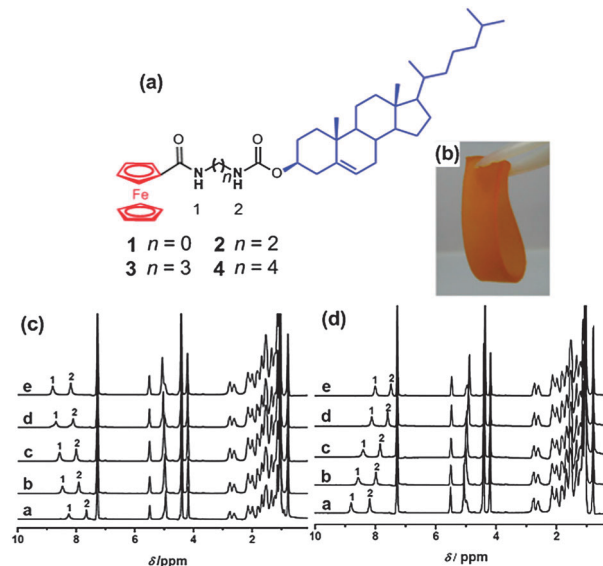


**Fig. 2** (a) Chemical structures of cholesterol-appended ferrocene derivatives **1–4**; (b) a photograph of a gel film of the **1**/cyclohexane system; (c) <sup>1</sup>H NMR spectra of **1** in C<sub>6</sub>D<sub>6</sub> at different concentrations (a, 30 mg mL<sup>-1</sup>; b, 35 mg mL<sup>-1</sup>; c, 40 mg mL<sup>-1</sup>; d, 45 mg mL<sup>-1</sup>; e, 50 mg mL<sup>-1</sup>); (d) <sup>1</sup>H NMR spectra of **1** (50 mg mL<sup>-1</sup>) in C<sub>6</sub>D<sub>6</sub> at different temperatures (a, 298 K; b, 303 K; c, 308 K; d, 318 K; e, 323 K) (reproduced with permission of John Wiley & Sons, Inc. from ref. 42).

on the basis of benzo-21-crown-7 constructed by orthogonal self-assembly.<sup>44</sup> The gel is sensitive to temperature. The reversible gel–sol transition can be achieved by heating and cooling. Temperature-dependent <sup>1</sup>H NMR spectra were conducted to provide convincing evidence for this gel–sol transition. The <sup>1</sup>H NMR signals for the gelator almost disappeared at a relatively low temperature, indicating strong intermolecular aggregation. The gel changed into a sol gradually with increasing the temperature, resulting in the appearance of the original well-dispersed signals.

However, <sup>1</sup>H NMR presents serious limitations in studying the interactions between the gelators in the gel state due to the reduction of the mobility. Generally, the gelators incorporated and immobilised within the “solid-like” network can not be monitored by <sup>1</sup>H NMR spectroscopy due to line broadening and loss of spectral resolution, while the gelators within the “liquid-like” solution phase have sharp NMR peaks as a consequence of its molecular-scale mobility.<sup>45,46</sup> Smith and coworkers utilized this simple NMR integration approach to calculate the relative content of gelators in the immobilised, “solid-like” gel network and liquid-like solution phases.<sup>47</sup> The optimal molar ratio was reasonably monitored to be 1 : 1 between *L*-lysine-based dendron and rigid diamines (1,4-diaminobenzene and 1,4-diaminocyclohexane) in the two-component gels. Self-organisation and component selection processes could also be observed when the dendron was mixed with an equimolar mixture of 1,2-, 1,3- and 1,4-diaminobenzene in 1 : 1 : 1 : 1 ratio. Furthermore, NMR relaxation measurements demonstrated that selective interactions could be achieved between the gel based on dendron/1,4-diaminobenzene and a ternary guest molecule pyrene.

High resolution magic angle spinning (HRMAS) NMR is especially useful for studying interfaces between a translationally

mobile liquid and an immobile or less mobile media (such as solid support, gel and microparticle) and for detecting NMR resonances from conformationally mobile chemical moieties that are grafted to or interacting with the immobile phase.<sup>48,49</sup> Escuder, Miravet, Willem *et al.* used HRMAS <sup>1</sup>H NMR for the conformational behaviour characterization of supramolecular gels derived from valine in order to gain insight into the structures and properties of the aggregates in the fibrillar network.<sup>50</sup> Diffusion filters were essential in order to eliminate the signals from non-aggregated molecules that were in equilibrium with the gel network. Notably, only the flexible parts in the gel state could be monitored by <sup>1</sup>H NMR spectroscopy because the polarities of acetonitrile (a polar solvent) and toluene (a rather non-polar solvent) played distinct roles in the determination of the mobility for the different moieties in the gelators. The dipolar interactions for the particular NMR signals related to the mobile moieties with sufficient isotropic rotational mobility (correlation time of *ca.* 10<sup>-11</sup> s or less) are eliminated when they are dipped in the non-viscous liquid phase, resulting in vanishing of the dipolar broadening exactly as in typical homogeneous liquid NMR.

## 2.2 Diffusion ordered NMR spectroscopy (DOSY)

Diffusion ordered NMR spectroscopy (DOSY) has become more and more important to investigate the self-assembly processes from building blocks to the formation of functional nanomaterials. DOSY shows its superiority in the characterization of objects with an intermediate dimension ranging from dozens of Ångströms to hundreds of nanometers. The translational self-diffusion coefficient ( $D_t$ ), which is difficult to obtain with other methods, can be derived from DOSY without any need to separate the mixtures of species.<sup>51-53</sup> This accounts for the net result of the thermal motion induced by random-walk processes experienced by particles or molecules in solution, in the absence of any chemical potential gradient. Based on the  $D_t$  values, accurate hydrodynamic dimensions (shape and size) of the aggregates can be obtained by using the Stokes–Einstein equation as well as the thermodynamic parameters (equilibrium constant and the  $\Delta G^0$  of the aggregative process) of the self-assembly processes.<sup>54</sup>

Huang and co-workers reported the formation of a supramolecular polymer driven by host–guest interactions between dibenzo-24-crown-8 (DB24C8) and dibenzylammonium salt (DBA) moieties on the basis of an AB-type heteroditopic monomer **5** (Fig. 3a).<sup>55</sup> Compared with the formation of monomers/oligomers in dilute solution, a linear supramolecular polymer formed at relatively high concentration firstly from the self-organization of **5**. These supramolecular polymers assembled into one-dimensional fibrils, which aggregated from long supramolecular polymer chains at first and subsequently form an entangled fiber network which prevented the flow of bulk solvent. Through the entanglement of supramolecular fibrils, three-dimensional fiber networks were constructed and macroscopic organogel finally formed by incorporating solvent molecules.

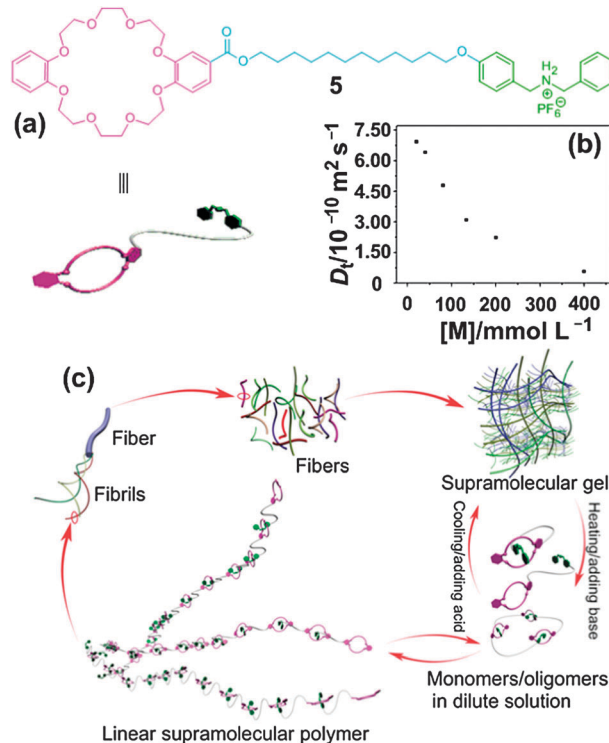


**Fig. 3** (a) Chemical structure of dibenzo-24-crown-8 based gelator **5**; (b) concentration dependence of diffusion coefficient  $D_t$  of the supramolecular polymer formed from self-organization of **5**; (c) cartoon representation of the formation of a supramolecular polymer gel via self-assembly of **5** in acetonitrile (reproduced with permission of John Wiley & Sons, Inc. from ref. 55).

Two-dimensional diffusion ordered NMR (DOSY) experiments were utilized to investigate the self-assembly process from the monomer to the supramolecular polymer. As the monomer concentration increased from 20 mM to 400 mM, the measured weighted average diffusion coefficient decreased considerably from  $(6.92 \pm 0.35) \times 10^{-10} \text{ m}^2 \text{ s}^{-1}$  to  $(5.62 \pm 0.28) \times 10^{-11} \text{ m}^2 \text{ s}^{-1}$  (Fig. 3b), indicating the supramolecular polymerization of monomer **5**. By increasing the concentration of **5**, the solution viscosity increased rapidly, so flow capacity of the solvent molecules in the bulk phase was limited efficiently, resulting in the rapid reduction of the  $D_t$  value. Based on the previous reports,<sup>56,57</sup> it was known that a high degree of polymerization value for the repeating unit is necessary to result in a 10-fold decrease in the diffusion coefficient. Hence, the DOSY experiments clearly indicated the formation of an extended, high molecular weight polymer structure.

It is generally known that the secondary ammonium salt group can be deprotonated by adding base, thus destroying the host–guest recognition between DB24C8 and DBA and making the complex disassemble.<sup>58-65</sup> The pH-responsive assembly and disassembly processes were also confirmed by <sup>1</sup>H NMR spectra. Hence, this supramolecular polymer gel has pH- and thermo-responsive abilities and good reversibility of gel–sol phase transitions induced by heating and cooling or by adding base (triethylamine) and acid (trifluoroacetic acid). This dual-responsive supramolecular polymer gel driven by crown ether

based molecular recognition is a promising model material for drug-delivery systems and other applications.

### 2.3 Nuclear Overhauser effect spectroscopy (NOESY) and rotating frame nuclear Overhauser effect spectroscopy (ROESY)

Two-dimensional nuclear magnetic resonance spectroscopy (2D NMR) is a set of methods which give data plotted in a space defined by two frequency axes rather than one. 2D NMR spectra can provide more information about a molecule than 1D NMR spectra and are especially useful in determining the structures of molecules, particularly for molecules that are too complicated to work out by using 1D NMR. In supramolecular chemistry, 2D NOESY is a useful tool to study the relative positions of building components in host-guest inclusion complexes.<sup>66–68</sup>

Harada and coworkers mixed curdlan ( $\beta$ -1,3 glucan) **6**, which is functionalized with  $\alpha$ -cyclodextrin ( $\alpha$ -CD), and an azobenzene modified poly(acrylic acid) **7** in 1 : 1 ratio of the monomer units in water to construct an interesting photoresponsive hydrogel based on a supramolecular polymer network (Fig. 4).<sup>69</sup> The size of the *trans* azo group is suitable for the cavity of  $\alpha$ -CD to form an inclusion complex, while the size of the *cis* state is too large to be wrapped by  $\alpha$ -CD, resulting in the disassembly of the inclusion complex.<sup>70–74</sup> Upon irradiation with UV light (365 nm), the hydrogel transformed into a sol due to the isomerization of the azo groups in **7** (*trans/cis* = 12 : 88), whereas visible light (430 nm) or heating (60 °C) can lead to the isomerization of the azo moieties from the *cis* state to the *trans* state (*trans/cis* = 75 : 25), resulting in the re-formation of the hydrogel within two minutes. The reversible formation of the supramolecular hydrogel could be repeatedly induced by using UV and visible light.

2D NOESY spectroscopy was utilized to confirm the threading/dethreading processes. Nuclear Overhauser effect (NOE) correlation peaks between the protons of the *trans*-azo group and the inner protons of the  $\alpha$ -CD unit were observed, indicating that the side chain of **7** was deeply included in the cavity of  $\alpha$ -CD in aqueous solution. When the gel transformed into the sol upon irradiation with UV light, no correlation peaks between the protons related to the *cis*-azo units and the  $\alpha$ -CD groups could be observed, which indicated the dissociation of the inclusion complexes.

Apart from the inclusion complexes, NOESY spectroscopy is also an effective method to investigate other supramolecular gel systems. Pérez-Pérez *et al.* constructed a novel organogelator incorporating asparagine and tryptophan residues which exhibited fluoride-responsiveness.<sup>75</sup> NOESY experiments were conducted both in the gel state and in solution (1 mM). Positive NOEs could be observed in solution with 500 ms mixing time, indicating the existence of aggregates with a long correlation time in solution. By contrast, the same experiment in the gel state was done with only 5 ms mixing time and showed opposite NOE signs, which were ascribed to a change of the conformation in the network or the contributions of intermolecular NOEs within the aggregates.

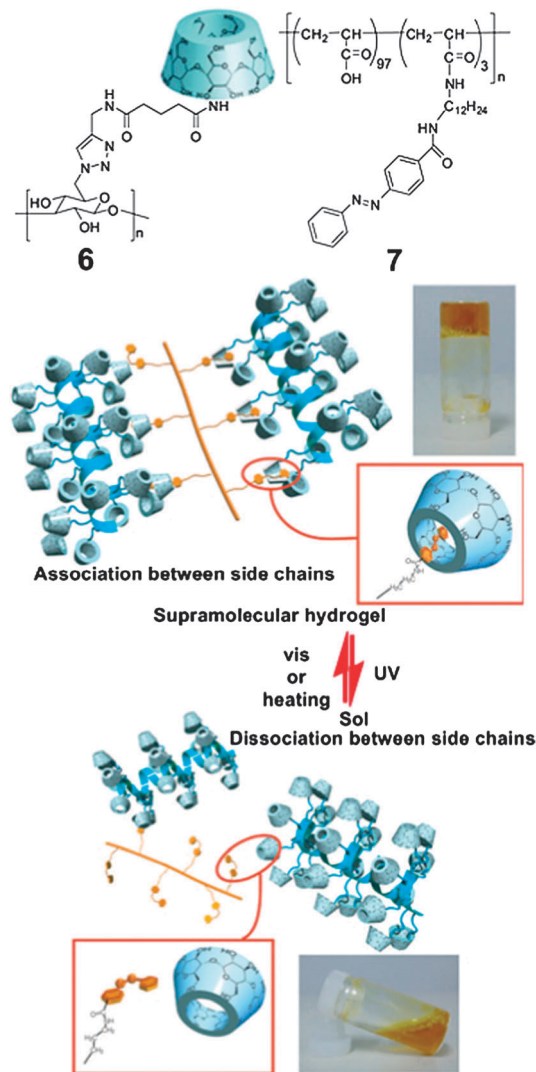


**Fig. 4** Chemical structures of host polymer **6** and guest polymer **7** and schematic representation of the photo-controlled interactions of the  $\alpha$ -CD unit with azobenzene moieties (reproduced with permission of John Wiley & Sons, Inc. from ref. 69).

ROESY is similar to NOESY, except that the initial state is different. Instead of observing cross relaxation from an initial state of  $z$ -magnetization related to NOESY, the equilibrium magnetization of ROESY is rotated onto the  $x$  axis and then spin-locked by an external magnetic field. The cross-relaxation rate constant is always positive in ROESY, which is quite different from that of NOESY, which goes from positive to negative as the correlation time increases, giving a range where it is near zero. This method is especially useful for certain molecules whose rotational correlation time fall in a range where the NOE is too weak to be detectable, usually molecules with a molecular weight around 1000 Daltons,<sup>76–78</sup> because ROESY has a different dependence between the correlation time and the cross-relaxation rate constant.

Harada and co-workers designed an ingenious supramolecular gelator *N*-(2,4,6-trinitrophenyl)-6-amino-transcinnamoyl- $\beta$ -CD (**9**), which was quite different from analogues **8** forming

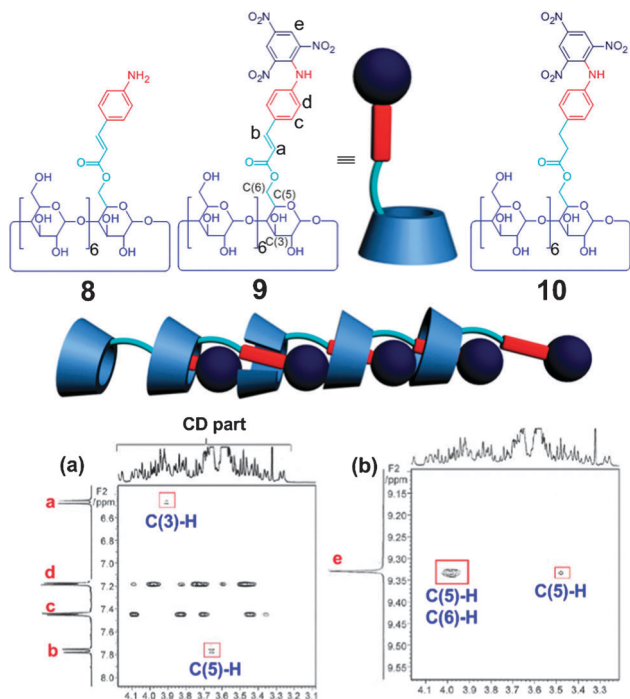


**Fig. 5** 2D ROESY  $^1\text{H}$  NMR spectra of **9** (5 mM,  $\text{D}_2\text{O}$ ,  $30\text{ }^\circ\text{C}$ ): (a) the correlations of the protons of the CD group with the protons of the cinnamoyl moiety; (b) the correlations of the protons of CD group with the protons of the TNB moiety (reproduced with permission of John Wiley & Sons, Inc. from ref. 79).

crystals in a tail-to-tail pattern from its super-saturated solution and **10** forming a precipitate when its super-saturated solution was cooled down (Fig. 5).<sup>79</sup> They found that modified CDs with flexible hydrocinnamic groups formed self-inclusion complexes in water, but the rigid cinnamic group inhibited the formation of an intramolecular complex.<sup>80</sup>

The 2D ROESY NMR spectra (Fig. 5) show the rotational NOE (ROE) interactions between the inner protons of the CD and both protons of the 2,4,6-trinitrophenyl (TNB) group and the cinnamic protons, thus indicating that these units penetrated into the CD cavities. The observed C(1)H protons were widely dispersed in the range from 4.8 to 5.5 ppm caused by the reduction of the modified  $\beta$ -CD after the formation of inclusion complexes between the substituent at the 6-position of the  $\beta$ -CD and the adjoining CD cavity. Protons a and b related to the cinnamoyl moiety showed strong correlations with the C(3)H and C(5)H protons of  $\beta$ -CD, respectively. On the other hand, strong correlations between the protons corresponding to the 2,4,6-trinitrophenyl ring and the C(5)H and C(6)H protons of  $\beta$ -CD were observed. These correlations confirmed the formation of the tail-to-head structure instead of a tail-to-tail structure.

Vapor pressure osmometry (VPO) measurements were also conducted to determine the molecular weight ( $M_w$ ) of this supramolecular system. The  $M_w$  value of the supramolecular polymer formed by **9** was about 16 000 (about 13 monomers) at 5 mM in aqueous solution, which indicated that the modified  $\beta$ -CD formed supramolecular fibrils as the initial step of supramolecular gelation.

### 3. Computational techniques

Computational approaches can be used to simulate molecular and atomic behavior based on fundamental descriptions of atomic and molecular orbitals (*ab initio* quantum mechanics), experimental data (*a priori* molecular mechanics, MM), or a combination of both (semiempirical methods). On the basis of the initial structure which comes from crystallographic studies, it is usual to use MM to get a guess of the equilibrium geometry. Then, other methods can be used to simulate a variety of possible structures. Thermochemical data and other simulated information can also be obtained from higher-level methods. It is crucial to gain insight into the noncovalent interactions leading to the gel formation from the molecular level. In most cases, we cannot get single crystal structures that can provide direct information about the interactions in the solid state. So, computational approaches play important roles in the investigation of interactions between the gelators, which can help us to understand the gelation mechanisms.<sup>81–84</sup> Possible modes of aggregation for gelators can be identified by using high level energy minimization and molecular dynamics calculations.

$\pi$ -Conjugated low-molecular organic gelators (LMOG) have attracted more and more attention of chemists over past decades because they assemble to produce photo- and electrochemically functional supramolecular assemblies.<sup>85–88</sup> Haino *et al.* systematically studied the self-assembly and gelation behaviors of tris(phenylisoxazolyl)benzene derivatives **11** (Fig. 6a).<sup>89</sup> The flat aromatic compound **11a** stacked in a columnar fashion along its  $C_3$  axis *via*  $\pi$ - $\pi$  stacking interactions. This gelator turned into a gel in both nonpolar and

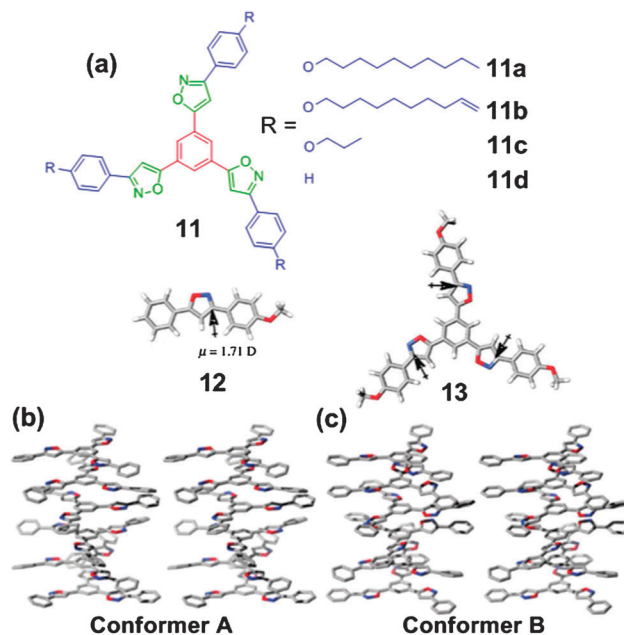


**Fig. 6** (a) Chemical structures of **11** and calculated geometries of **12** and **13** by DFT method using B3LYP/6-31G\*. Stereo plots of two local minimum geometries for the hexameric **11d** obtained from conformation search by MacroModel program: (b) helical arrangement of the local dipoles; (c) anti parallel arrangement of them (reproduced with permission of American Chemical Society from ref. 89).

highly polar solvents such as methylcyclohexane, ether, acetone, dimethylsulfoxide, *etc.* Compound **11b** with the unsaturated termini impedes the intermolecular association, resulting in the reduction of the gel stability, while compound **11c** with shorter alkyl chains is not efficient for the gelation. Furthermore, the absence of a peripheral alkyl chain and branched chain structure (**11d**) remove the gelation ability.

Theoretical calculation of the self-assembled behaviors provides important evidence that complements the experimental studies in solution. The DFT method (B3LYP/6-31G\*) was chosen for theoretical calculations by using 1,3,5-tris[3-(4-methoxyphenyl)isoxazol-5-yl]benzene (**13**) and its partial structure, 3-(4-methoxyphenyl)-5-phenylisoxazole (**12**) as model compounds. From the calculation, it was found that compound **12** has a quite large dipole moment ( $\mu = 1.71\text{D}$ ). The local dipole-dipole interactions among the three isoxazole rings of **13** enable them to adopt a circular array, which regulate the arrangement of the resultant self-assembly. The barrier to flip one of the isoxazole rings to the opposite direction was calculated to be  $\Delta E = 1.00 \text{ kcal mol}^{-1}$ .

A conformational study of the hexameric assembly of **11d** was also conducted as a model system (MMFF94s) to investigate the possible structures of the supramolecular self-assemblies. Two major geometries (Fig 6b and c) were obtained within  $1.0 \text{ kcal mol}^{-1}$ . In conformer A, the local dipoles align in a head-to-tail manner, which makes it adopt a helical geometry. While conformer B is achiral, the reason is that due to the attractive antiparallel orientation of the local dipoles, the phenylisoxazolyl groups adopt an unusually eclipsed geometry, which produces molecular pairs, built up as piles in a staggered manner. These two conformers can exist in solution; the presence of chiral conformer A leads to an achiral environment wherein the helical sense of conformer A can be biased by the addition of chiral stimuli.

Coarse grain model is another useful molecular simulation technique that can provide significant information (such as aggregate size distribution, polydispersity of aggregates, internal energy and heat capacity) about the self-assemblies of complex molecules which play crucial roles in the formation of supramolecular gels.<sup>90</sup> For example, de la Cruz *et al.* employed this method to investigate the self-assembly of a peptide amphiphile molecule driven mainly by hydrophobic interactions between alkyl tails and hydrogen bonds between peptide blocks.<sup>91</sup>

## 4. X-Ray techniques

Over the past 15 years, significant advances in X-ray techniques have completely transformed how chemists make use of this technique. This is particularly evident in the field of supramolecular chemistry, where characterizing the structural motifs of molecular crystals is crucial for understanding the weak intermolecular forces that are responsible for crystal stability.<sup>92</sup>

### 4.1 Single-crystal diffraction

X-ray crystallography has led to a better understanding of chemical bonds and noncovalent interactions. X-ray crystallography

is a method of determining the arrangement of atoms within a crystal, in which a beam of X-rays strikes a crystal and causes the beam of light to spread into many specific directions. From the angles and intensities of these diffracted beams, a crystallographer can produce a three-dimensional picture of the density of electrons within the crystal. From this electron density, the mean positions of the atoms in the crystal can be determined, as well as their chemical bonds, their disorder and other information. X-ray crystal structures can also account for unusual electronic or elastic properties of a material, shed light on chemical interactions and processes, or serve as the basis for designing pharmaceuticals against diseases.<sup>93–96</sup>

Kim *et al.* elegantly utilized cucurbit[7]uril (CB[7]) without any modification of its periphery to construct a simple macrocyclic, pH-triggered hydrogelator (Fig. 7).<sup>97</sup> This gel not only is sensitive to external stimuli but also shows unprecedented guest-induced stimuli-responsive behavior.

The  $pK_a$  value of CB[7] is measured to be 2.2, which was little higher than the optimum pH value for the gel formation (0–2), suggesting that the complexation of hydrogens to the CB[7] portals play a significant role on the hydrogel formation. X-ray crystal structure of CB[7] grown from a solution with a low concentration of CB[7] (*ca.* 1 wt%) provided direct evidence for the formation of the hydrogel. In the crystal structure, the CB[7] molecules are packed in a herringbone structure along the *a* axis. On the *ab* plane, each CB[7] molecule can interact with six neighboring CB[7] molecules through extensive C-H...O hydrogen bonds. Furthermore, water molecules and/or hydronium ions act as a “glue” to connect CB[7] molecules to form an approximately 11 nm long secondary building unit, which assembles into a long fibril. The fibrils then bundle into a thick fiber, which forms a 3D network leading to the hydrogel formation.

### 4.2 Small-angle X-ray scattering

X-ray scattering techniques are non-destructive and can reveal information about the crystal structure, chemical composition,

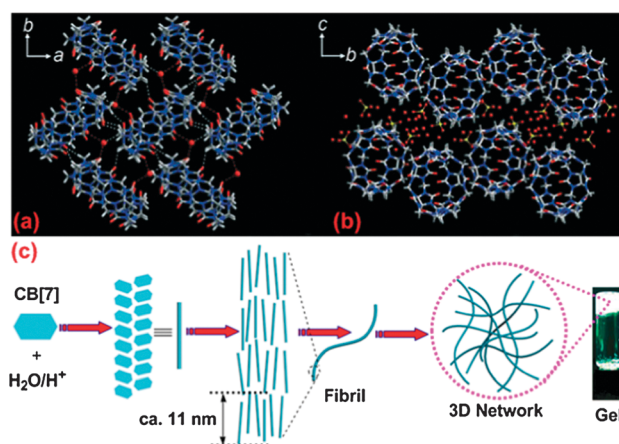


**Fig. 7** X-ray crystal structure of CB[7]. Color codes: gray C, blue N, red O, yellow S, white H. (a) Organization of CB[7] molecules on the *ab* plane. (b) A packing diagram on the *bc* plane. (c) Cartoon representation of the hydrogel formation (reproduced with permission of John Wiley & Sons, Inc. from ref. 97).

and physical properties of materials and thin films. These techniques are based on observing the scattered intensity of an X-ray beam hitting a sample as a function of incident and scattered angle, polarization, and wavelength or energy.

Small-angle X-ray scattering (SAXS), one of these techniques, probes structures in the nanometer to micrometer range of supramolecular assemblies by measuring scattering intensity at scattering angles ( $2\theta$ ) close to  $0^\circ$ . Traditionally, SAXS is employed to acquire key parameters of the aggregates, such as the molecular weight ( $M_w$ ), radius of gyration ( $R_g$ ), and maximum intramolecular distance ( $D_{\max}$ ), average particle size, shape, distribution, and surface-to-volume ratio.<sup>98</sup>

SAXS is used widely for studies of colloids of all types, metals, cement, oil, polymers, plastics, proteins, foods and pharmaceuticals. Since most of supramolecular gels contain fiber-like structures interconnected by multiple non-covalent interactions, SAXS is especially useful to characterize the shape, size, and distribution of these fibers. On the other hand, the packing mode can also be derived from SAXS results.<sup>99–101</sup>

Smith and coworkers reported novel one-component gelators comprising L-lysine-based dendritic headgroups with different generations (from first to third) covalently connected to aliphatic diamine spacer chains of different lengths *via* an amide bond (Fig. 8).<sup>102</sup> Intermolecular hydrogen bonds between the amide groups are the primary driving forces directing the self-assembly process that underpins macroscopic gelation, with the carbamates in the dendritic headgroups playing a supporting or secondary role. These gelators exhibited a positive dendritic effect, additional hydrogen bonds possible for the higher generation systems played significant roles on the thermal properties of gels up to the third generation.

Gelator **G1–C12–G1** self-assembled into “sausage-like” morphologies with the thickness of *ca.* 120 nm, which grew unidirectionally. Compared with **G1** with lower generation dendrimers, **G2** and **G3** form more efficient interpenetrated sample-spanning networks. To probe the morphologies observed by SEM, SAXS was utilized. Fig. 8a and b showed the results obtained for the modeling of the SAXS curves for **G1–C12–G1** at 25 and 47 °C. Although the scattering profiles were different at the two temperatures, the average radius ( $R_c$ ) of the self-assemblies, modeled as infinite solid cylinders, remained the same at 72 Å, which were in good agreement with the morphology observed by SEM. These SAXS data provided convincing evidence for the formation of a sausage-like morphology with relatively large nanoscale features. On the other hand, it revealed that the polydispersity grows from 3.2% to 3.6% for **G1–C12–G1** upon increasing the temperature. As shown in Fig. 8c, the  $R_c$  value for **G2–C12–G2** at 22 °C was determined to be about 17.5 Å with a polydispersity of 9%, which was similar to the expected dimensions of **G2–C12–G2**. This result suggested that the gelator **G2–C12–G2** self-assembled into cylinder-like anisotropic objects with the width of a single dendrimer building block.

### 4.3 Wide-angle X-ray scattering (WAXS)

Wide-angle X-ray scattering (or powder diffraction) is almost the same technique as small-angle X-ray scattering (SAXS).

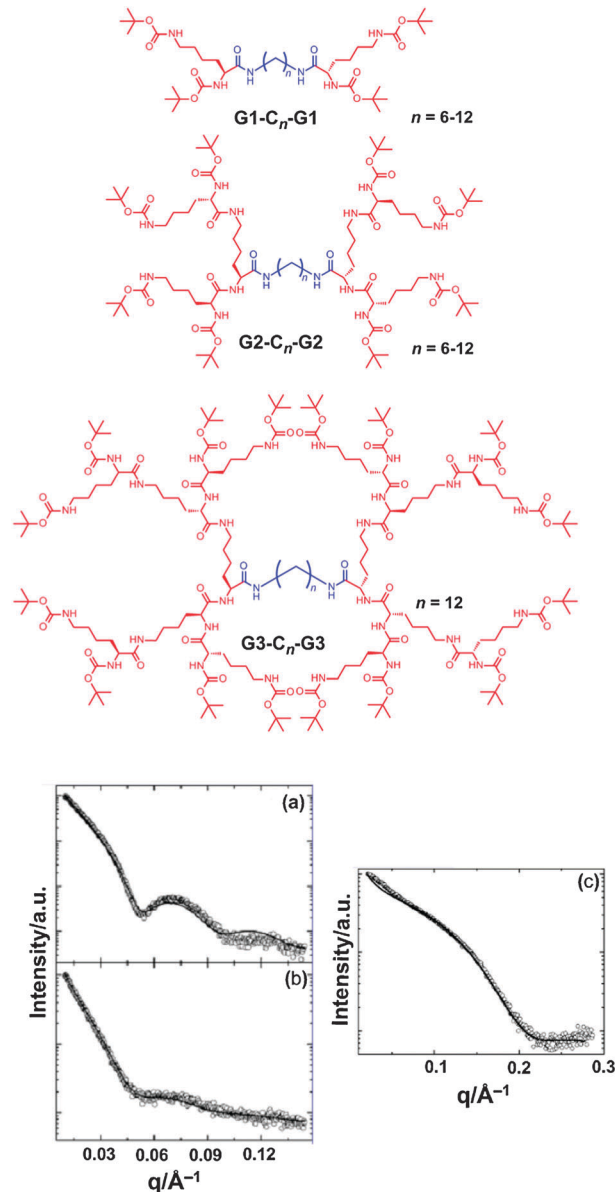


**Fig. 8** SAXS data for **G1–C12–G1** at (a) 25 °C and (b) 47 °C; (c) SAXS data for **G2–C12–G2** at 22 °C (reproduced with permission of American Chemical Society from ref. 102).

The only difference is that the distance from the sample to the detector for WAXS is shorter than that of SAXS and thus diffraction maxima at larger angles are observed. This technique specifically refers to the analysis of Bragg peaks scattered to wide angles ( $2\theta$  larger than  $5^\circ$ ), which implies that they are caused by sub-nanometer-sized structures (by Bragg's law).<sup>103</sup>

This technique is a time-honored but a somewhat out-of-favor technique for the determination of degree of crystallinity of polymer samples. The diffraction pattern generated allows the determination of chemical composition, texture or phase composition of the film, crystallite size and presence of film stress. A crystalline solid consists of regularly spaced atoms (electrons) that can be described by imaginary planes. The distance between these planes is defined as the *d*-spacing.

The intensity of the  $d$ -space pattern is directly proportional to the number of electrons (atoms) that are found in the imaginary planes. Every crystalline solid will have a unique pattern of  $d$ -spacings (the powder pattern), which is a “finger print” for that solid. In fact, solids with the same chemical composition but different phases can be identified by their pattern of  $d$ -spacings. Therefore, WAXS is an effective method to confirm the packing modes of the gelators in the solid state.<sup>104–108</sup>

It should be noted that there are many differences between the data extracted from the gel state (very broad X-ray scattering features) and those obtained from the solid state (much sharper crystalline-like features). The reason is that gels have solid-like rheology and do not flow, but the solvent is still the major component. In addition, the packing mode of the molecules in the gel state differs from that in the solid state, even in the crystalline phase.

The urea functionality has been widely incorporated into low-molecular-weight organogelators because it provides a convenient 1D directionality and strong intermolecular hydrogen-bonding interactions.<sup>109–113</sup> Miravet and co-workers designed a super-gelator containing chiral bisurea units (**14**) which can form hydrogels at very low concentration (Fig. 9).<sup>114</sup>

Wide-angle X-ray powder diffraction (WAXD) was used to investigate the structure of the dried hydrogels (xerogels) of bisurea **14** ( $R$  and  $S$ ). Information about the molecular packing mode of gelator molecules in neat gels can be obtained from an X-ray diffraction pattern of the xerogel. For  $R$ -**14**, the xerogel showed a high degree of crystallinity. The diffraction pattern is characterized by four sharp reflection peaks of 21.01, 10.64, 7.13, and 5.37 Å (Fig. 9d), the relative intensity of which is almost exactly in the ratio of 1:1/2:1/3:1/4:1, suggesting a lamellar organization. The low-angle peak ( $2\theta = 4.2^\circ$ ) corresponds to the extended molecular dimension, and a model with the packing can be proposed in which chiral columnar stacks are packed into a layered structure. The packing pattern of enantiomer  $S$ -**14** in the gel state was similar to  $R$ -**14**, shown in Fig. 9e. WAXD results provided convincing evidence for the presence of microcrystalline fibers in the wet gel, which could be demonstrated by TEM.

#### 4.4 Small-angle neutron scattering

Small-angle neutron scattering (SANS) is an experimental technique that uses elastic neutron scattering at small scattering angles to investigate the structure of various substances at a mesoscopic scale ranging from 1 to 1000 nm.

SANS usually uses collimation of a neutron beam to determine the scattering angle, which results in an ever lower signal-to-noise ratio for data that contains information on the properties of a sample at relatively long length scales ( $> 1 \mu\text{m}$ ).<sup>115</sup> Exchanging between hydrogen and deuterium always has a minimal effect on the sample, whereas it has dramatic effects on the scattering. SANS just relies on the differential scattering of hydrogens vs deuteriums.

SANS is very similar to SAXS in many respects. Both techniques are jointly referred to as small-angle scattering (SAS). During a SANS experiment, a beam of neutrons is directed at

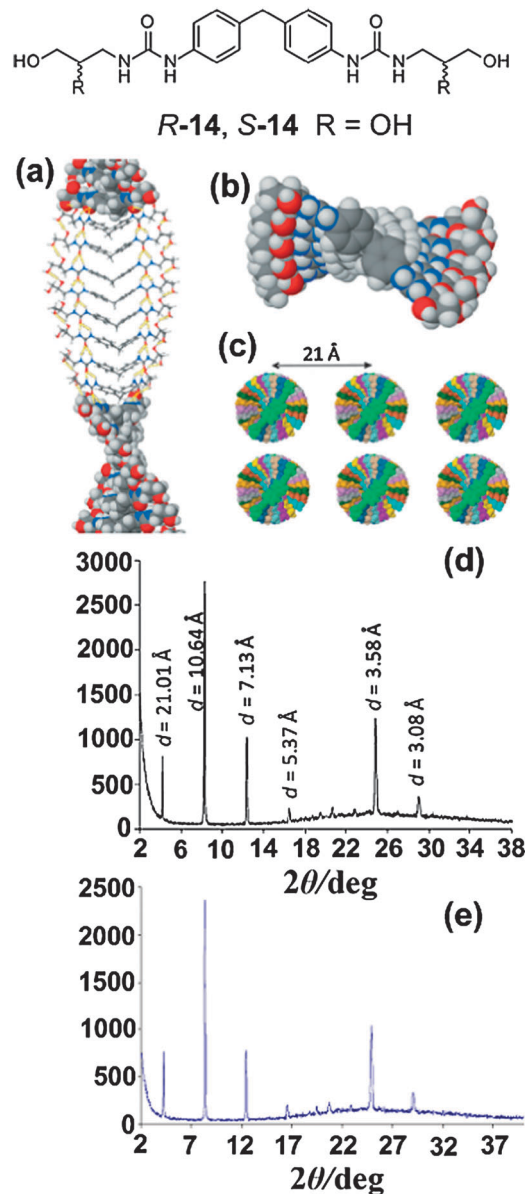


**Fig. 9** (a, b) Model of the proposed self-assembly process for hydrogelator **14** (c: inter-columnar packing). WAXD of the xerogels: (d)  $R$ -**14**; (e)  $S$ -**14** (reproduced with permission of John Wiley & Sons, Inc. from ref. 114).

a sample, and the neutrons are elastically scattered by nuclear interaction with the nuclei or interaction with the magnetic moments of unpaired electrons, while in X-ray scattering, photons interact with electron clouds. Advantages of SANS over SAXS are its sensitivity to light elements, the possibility of isotope labelling, and the strong scattering by magnetic moments.<sup>116</sup>

Organic–inorganic hybrid materials have attracted increasing attention over past decades due to their excellent processability and properties that can differ enormously from those of their separate parts.<sup>117–120</sup> Weiss and co-workers utilized an Fe(III) complex with phosphorus-containing amphiphile **15** as a two-component isothermal gelator to construct an organogel,<sup>121</sup> in which gelation can be induced isothermally (Fig. 10). The phosphorus-containing “latent” gelator binds to the Fe(III) ion

rapidly *in situ* accompanied by polymerization to form self-assembled fibrillar gel networks consisting of linear aggregates in the form of giant inverted micellar rods with narrow cross-sections. A variety of techniques were employed to gain insights into the structure of the gelator-iron(III) complex as well as the mechanism of its formation and the gelation process. It was found that only two oxygen atoms of the phosphate diester were involved in the complexation with Fe(III), and the complexation occurred very rapidly upon addition of Fe(III), while the aggregation of the complex into inverted cylindrical micelles occurred more slowly.

SANS provided information about the structure on the nanoscale involved in the networks of the **15**/Fe(III) complex in gel. It showed that the cross-sectional radii of the cylindrical fibers were around 15 Å, which confirmed that the gel was made up of long and rigid fibrillar species. On the other hand, a “plateau-like” regime of the intensity decayed within one decade of the intermediary  $Q$  range ( $0.007 \text{ \AA}^{-1} < Q < 0.07 \text{ \AA}^{-1}$ ) was observed (Fig. 10b), indicating the presence of long and rigid fibers in the gels. Furthermore, sharp decay and a broad oscillation at larger  $Q$  are typical features of fibrillar scatterers.

The sharp and intense very low- $Q$  component revealed the presence of large-scale heterogeneities in the gel networks. Compared with the gel prepared in the deuterated toluene, the gel prepared in the deuterated dodecane showed much larger volume fraction in the SANS curves (curves 1 and 3 in Fig. 10b). The  $Q$ -separation in the scattering curve between the form factor signal and the low- $Q$  extra-intensity might result from the presence of small cross-sectional dimensions between

the fibers, which was supported by the presence of an intensity oscillation (maximum at *ca.*  $0.30 \text{ \AA}^{-1}$ ) and Guinier analysis.

From the analysis of the data of Fig. 10b, it was found that crystalline-like heterogeneities with poorly ordered periodicities in the 18–21 Å range existed in the gel. The distances for the neat complexes in lamellae determined by X-ray diffraction were different from those for complexes in the gel calculated by SANS ( $\sim 30 \text{ \AA}$ ). The length of the extended molecule **15** was calculated to be 26.7 Å, indicating that the long alkyl chains in the complex of Fe(III)  $\supset$  **15** were in extensively bent conformations.

## 5. Spectroscopy

### 5.1 Infrared spectroscopy

Infrared spectroscopy (IR) deals with the infrared region of the electromagnetic spectrum, which is light with a longer wavelength and lower frequency than visible light.<sup>122</sup> Infrared spectroscopy is a simple and reliable technique widely used in both organic and inorganic chemistry, in research, and in industry. It is widely used in quality control, dynamic measurements, and monitoring applications. Of course, IR can be utilized to characterize the formation process of supramolecular gels because it can provide an insight into the assembly of molecular scale building blocks and allow the determination of the noncovalent interactions responsible for gelation.<sup>123,124</sup>

Escuder and Miravet *et al.* reported a fascinating hydrogel on the basis of bolaform amino acid derived from L-valine (**16**). In this system, the entropy change associated with the hydrophobic effect is the driving force for the aggregation.<sup>125</sup> Interestingly, this gelator self-assembled into fibrillar networks in water with quite low or zero enthalpic component, while the entropy is favorable, because the hydrophobic effect is dominant in the self-assembly. The low enthalpy values are attributed to the result of a compensation of the favorable intermolecular hydrogen-bond formation and the unfavorable enthalpy component of the hydrophobic effect. Moreover, the gelation efficiency was easily improved by introducing groups with enhanced hydrophobicity into the molecules.

Studies by temperature-dependent IR spectroscopy revealed that intermolecular hydrogen bonding also played important roles in the aggregation process of **16** in water. As shown in Fig. 11a, new bands at  $1625 \text{ cm}^{-1}$  corresponding to the C=O group could be observed upon cooling a solution of **16**, indicating the formation of intermolecular hydrogen bonds as the aggregation took place. On the other hand, upon increasing the percentage of water, the C=O stretching shifted to lower wavenumbers, which also confirmed the formation of hydrogen bonds in the aggregation process. Furthermore, the bands related to the CH stretching region shifted to lower wavenumbers as the concentration increased due to the packing of aliphatic chains (Fig. 11b).

### 5.2 Ultraviolet-visible spectroscopy

Ultraviolet-visible spectroscopy (UV/Vis) refers to absorption spectroscopy or reflectance spectroscopy in the ultraviolet-visible

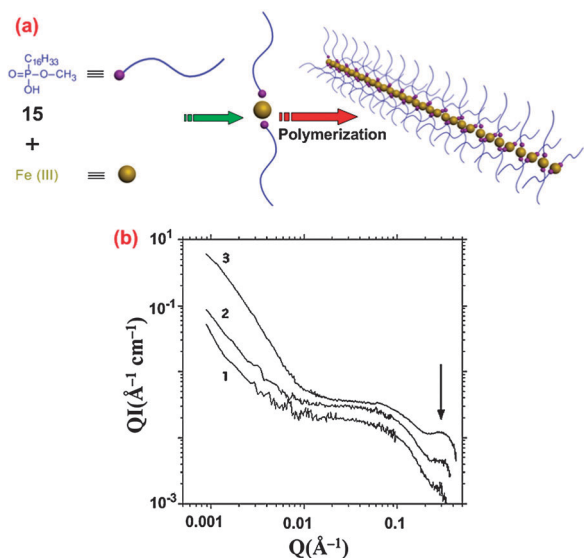


**Fig. 10** (a) Cartoon representation of a giant wormlike micelle formed upon complexation of *n*-alkyl monophosphonate esters with Fe(III) ions. The purple spheres are phosphonate headgroups attached to a long alkyl chain and metal ions are the yellow spheres. (b) Holtzer representations of scattering data at 24 °C for gels consisting of (1) 2.07 wt% **15**/MO-86 in toluene- $d_8$  and 2.9 wt%  $D_2O$ , (2) 1.0 wt% **15**/MO-86 in toluene- $d_8$  and 1.9 wt%  $D_2O$ , and (3) 1.0 wt% **15**/MO-86 in *n*-dodecane- $d_{26}$  and 9 wt%  $D_2O$  (reproduced with permission of American Chemical Society from ref. 121).

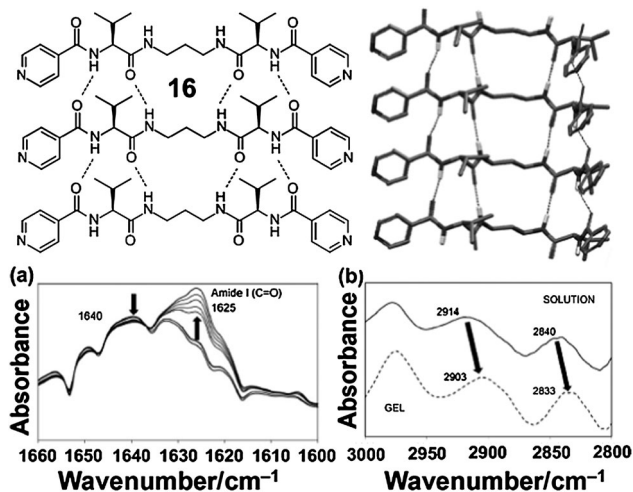


**Fig. 11** Schematic aggregation model of **16** and molecular mechanics energy minimized model. (a) Variation of the FTIR spectrum of a hot solution of **16** (14.5 mM) in water upon cooling to room temperature. Arrows indicate how the signals change with time. (b) FTIR spectra of compound **16** in D<sub>2</sub>O: solution (8 mM) and gel (14.5 mM) (reproduced with permission of John Wiley & Sons, Inc. from ref. 125).

spectral region. In this region of the electromagnetic spectrum, molecules undergo electronic transitions. This technique is complementary to fluorescence spectroscopy, since fluorescence deals with transitions from the excited state to the ground state, while absorption measures transitions from the ground state to the excited state.

Molecules containing  $\pi$ -electrons or non-bonding electrons ( $n$ -electrons) can absorb the energy in the form of ultraviolet or visible light to excite these electrons to higher anti-bonding molecular orbitals. The more easily the electrons can be excited (the lower the energy gap between the HOMO and the LUMO), the longer wavelength of light they absorb. UV/Vis spectroscopy is routinely used for the quantitative determination of different analytes, such as transition metal ions, highly conjugated organic compounds, and biological macromolecules.<sup>126</sup> UV/Vis spectroscopy is also widely used in the characterization of supramolecular gels because it can catch the changes in the hydrophobicity of the surroundings of a particular group which is part of the gelator and identify the noncovalent interactions.<sup>127–134</sup>

Miyata and Hisaki *et al.* designed a novel organogelator derived from boomerang-shaped dehydrobenzoannulenes with methyl ester groups (**17**) in *syn* positions (Fig. 12).<sup>135</sup> Highly-polarized substituents were introduced in the periphery to increase intermolecular affinity, and the molecule can be asymmetrized into a curved shape to align the molecules anisotropically and exclusively in a certain direction.

Temperature-dependent UV/Vis spectra of **17** in 1,2-dichloroethane evidenced gel formation and the molecular arrangement at a concentration of  $5.0 \times 10^{-3}$  M, which was higher than the CGC value ( $3.9 \times 10^{-3}$  M). When the temperature increased from  $-5$  to  $40$  °C, the gel degenerated gradually. As shown in the UV/Vis spectra, the intensity of the absorption bands ranging

from 345 to 440 nm increased along with the temperature rise, indicating that an aggregate formed by  $\pi$ - $\pi$  interactions between the annulene rings. On the other hand, the weak shoulder at about 510 nm decayed gradually, and the band at 484 nm became less discernable. The decreasing band was attributed to the energetically favored supramolecular structure in the gel, while the increasing band was ascribable to the monomeric species. By plotting the absorbance intensities at 355, 372, 440, and 510 nm *versus* temperature (Fig. 12a, inset), the  $T_g$  value could be obtained ( $32$  °C). On the contrary, these spectral changes could not be observed in the sol state when the concentration of **17** was lower than the CGC value ( $5.0 \times 10^{-4}$  M). The gelation process is depicted in Fig. 12c; boomerang-shaped gelators stack along a certain direction through dipole-dipole and  $\pi$ - $\pi$  stacking interactions. Due to the existence of effective dipole-dipole interactions, elongation took place in the  $\pi$ -stacking direction to yield a 1D fibrous superstructure. Then, the fibers constructed a 3D network to form the gel.

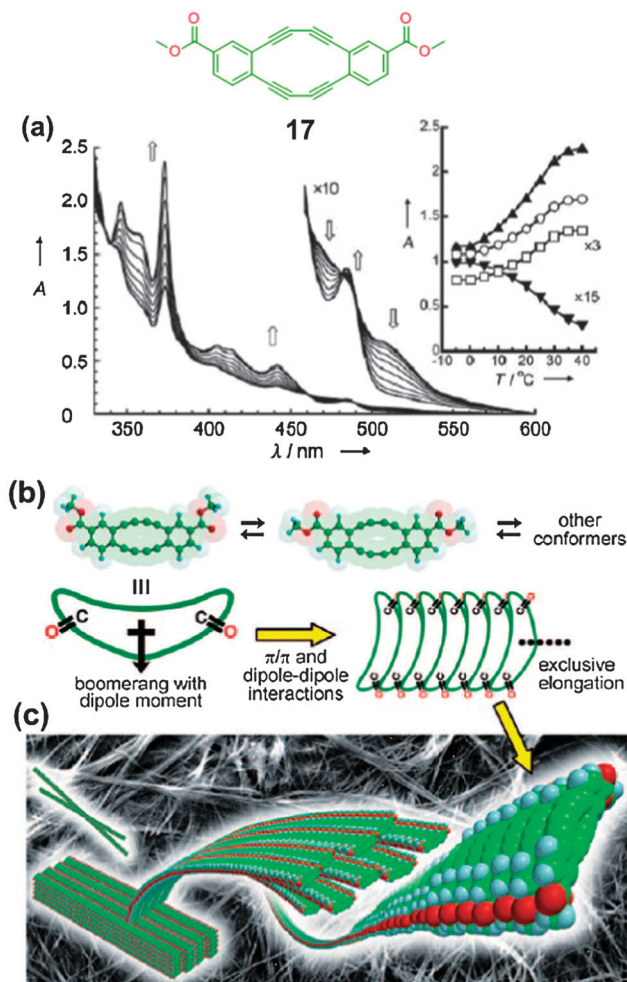


**Fig. 12** (a) UV/Vis spectra of **17** in 1,2-dichloroethane recorded at various temperatures ( $-5$  to  $40$  °C) at a concentration of  $5.0 \times 10^{-3}$  M. Inset shows absorbance changes at 355 (○), 372 (▲), 440 (□), and 510 (▼) nm. (b) Representation of the formation of the 1D columnar superstructure by the boomerang-shaped molecules. (c) The proposed superstructure in the gel of **17** (reproduced with permission of John Wiley & Sons, Inc. from ref. 135).

Zhang and Zhu *et al.* subtly designed a multi-stimuli responsive organogelator containing electroactive tetrathiafulvalene (TTF) and photoresponsive azobenzene groups.<sup>136</sup> This organogel responded not only to thermal stimuli but also to redox reactions and light irradiation. The gel–sol transition for this organogel could be reversibly changed by either chemical or electrochemical oxidation–reduction reactions of the TTF group. On the other hand, the gel–sol transition could also be achieved by photoisomerization of the azobenzene group in the gelator. The reversible *trans*–*cis* isomerization of the azo group controlled by UV and visible lights could be efficiently monitored by UV/Vis spectra.

### 5.3 Fluorescence spectroscopy

Fluorescence spectroscopy is another type of electromagnetic spectroscopy which analyzes fluorescence from a sample. Fluorescence spectroscopy is widely used in biochemical, medical, and chemical research fields for analyzing organic compounds.<sup>137</sup> It involves using a beam of light, usually ultraviolet light, that excites the electrons and causes them to emit light, typically, but not necessarily, visible light.

In fluorescence spectroscopy, the species is first excited, by absorbing a photon, from its ground electronic state to one of the various vibrational states in the excited electronic state. Collisions with other molecules cause the excited molecule to lose vibrational energy until it reaches the lowest vibrational state of the singlet excited electronic state. This process is often visualized with a Jablonski diagram. Then, the molecule drops down to one of the various vibrational levels of the ground electronic state again, accompanied by emission of a photon. As molecules drop down onto any of several vibrational levels in the ground state, the emitted photons will have different energies, namely, frequencies. Therefore, by analysing the different frequencies of light emitted in fluorescent spectroscopy, along with their relative intensities, the structures with different vibrational levels can be determined.<sup>138–143</sup>

Das and co-workers reported a novel donor–acceptor-substituted amphiphilic butadiene derivative (**18**) that can undergo spontaneous concentration-dependent hierarchical self-assembly from vesicles to gel, associated with unique changes in the fluorescence of the system (Fig. 13).<sup>144</sup> Due to the presence of a photoisomerizable chromophore in the gelator, **18** shows photo-responsive properties. A hierarchical build-up of supramolecular aggregates started from small-size vesicles. Then, these small vesicles adhere together to form larger vesicles at intermediate concentrations. Finally, a supramolecular gel with a continuous globular network forms.

Temperature-dependent absorption and emission spectroscopies were conducted to investigate the self-assembly of **18**. As shown in the absorption spectra (Fig. 13b), the intensity of the main peak at 432 nm decreased, while the absorption at 330 nm increased significantly when the temperature was reduced from 45 to 11 °C. The temperature-dependent changes in the absorption spectrum were also observed in its fluorescence spectra. The fluorescence intensity of the solution was dramatically enhanced (40-fold) upon reduction of the temper-

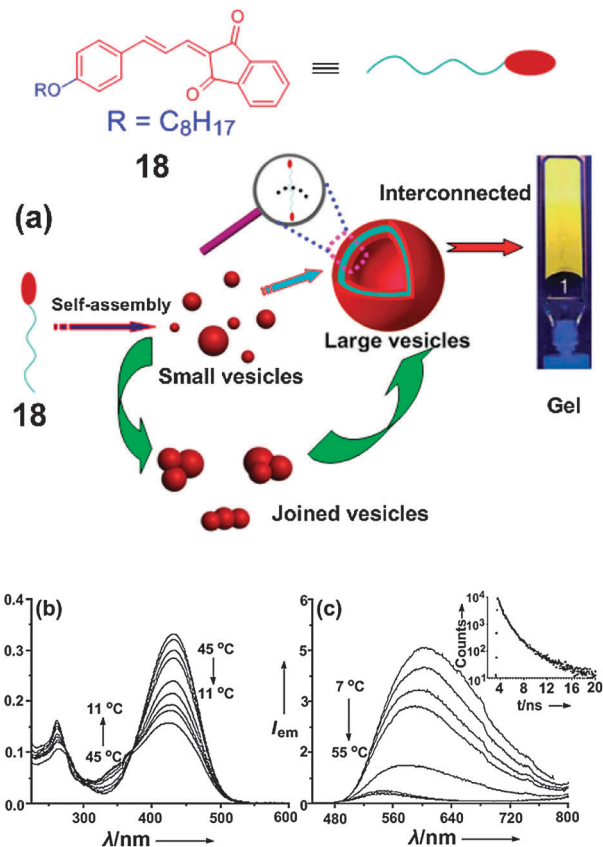


**Fig. 13** (a) Schematic representation of the hierarchical organization from small to large vesicles and finally to gels. The molecular self-assembly of only one bilayer is indicated. Temperature-dependent changes in (b) absorption ( $l = 1$  mm) and (c) emission spectra ( $\lambda_{\text{ex}} = 370$  nm;  $1 \times 1$  cm) of a  $1.2 \times 10^{-4}$  M solution of **18** in methanol. The inset shows the fluorescence decay profile monitored at 13 °C ( $\lambda_{\text{ex}} = 375$  nm;  $\lambda_{\text{em}} = 600$  nm) (reproduced with permission of John Wiley & Sons, Inc. from ref. 144).

ature from 55 to 7 °C, and the maximum band red-shifted from 540 nm to 602 nm. Notably, the lifetime of the species was observed to be 1.0 ns at 13 °C, which was much longer than that at 40 °C (<100 ps). Reversible phenomena can be monitored by increasing the temperature. These phenomena resulted from the formation of H aggregates, which involves a parallel stacking pattern of the chromophores. Compared with the monomer absorption band, the absorption in this system is dominated by the high-energy band, resulting in a blue shift in this system, while long-lived and strongly red-shifted fluorescence occurs due to the low-energy band.<sup>145</sup>

Tian and coworkers masterfully designed a photochromic fluorescent organogelator bearing bisthiénylene bridged fluorescent chromophore naphthalimide units.<sup>146</sup> This novel photochromic gelator exhibited excellent reversible photochromic behaviour in the gel state. The colour of the gel changed from yellow to red upon irradiation with UV light at 365 nm. Upon subsequent irradiation of the red gel with visible light ( $\lambda > 510$  nm), the system gradually returned to the initial status. The reason was that the bisthiénylene unit in the gelator underwent a reversible photochromic reaction. The cyclization and cycloreversion of the photochromic unit was

reversibly controlled by UV and visible light. The reversible spectral changes monitored by absorption and fluorescence spectra provided convincing evidence of the transformation between closed and open forms of the bisthiénylene unit.

#### 5.4 Circular dichroism spectroscopy

Circular dichroism (CD) refers to the differential absorption of left and right circularly polarized light. CD is one of the most convenient techniques in the study of the stereostructures and the intra- and intermolecular interactions of various classes of chiral supramolecules. CD is a very sensitive, destruction-free, and rapid instrumental method that requires typically submicrogram-scale sample to learn about intramolecular and intermolecular interactions of self-assembled systems, host-guest systems, polymers, and so on. Its higher sensitivity to molecular conformation and configuration makes CD spectroscopy a more powerful tool in the structural analysis of various chiral supramolecular systems than its parent achiral absorption spectroscopies such as ultraviolet (UV), visible (vis), and infrared (IR) spectra.<sup>132</sup> Due to these advantages, CD spectroscopy has a wide range of applications in many different fields, such as structural studies of small organic molecules, DNA, and proteins.

When an achiral sample is exposed to both right- and left-handed circularly polarised light, it can absorb both polarisations of light equally, resulting in a 'zero' spectrum. On the contrary, a chiral molecule absorbs the two polarisations differently, hence giving rise to a spectrum (either positive or negative). For the enantiomeric molecules, they exhibit CD spectra with equal and opposite signs. Mostly, the CD spectra of isolated molecules have relatively low ellipticities, while the chirality is sometimes expressed at a much larger scale in the morphology of self-assembled fibers. In supramolecular gel systems, many of the molecules commonly employed as gelators containing chiral centres. The chiral information at the molecular scale can be translated into gel-phase assemblies ranging from nanometers to micrometers *via* hierarchical assembly.<sup>147–150</sup> Hence, CD spectroscopy is an efficient method which can provide key insight into the assembly of gelator molecules into nanoscale chiral supramolecular objects.<sup>151–159</sup> Notably, variable temperature CD spectroscopy is always utilized to investigate the formation of nanoscale chiral aggregates owing to the thermal responsiveness of self-assembled fibres.

Conformational preferences of the amino acids determine peptide secondary and tertiary structure and play an important role in protein functions. Misfolding of the peptidic chain may produce unwanted processes that provoke fatal diseases.<sup>160</sup> Miravet and Escuder *et al.* reported a supramolecular gel formed by a low molecular weight peptidomimetic (**19**) containing a Pro-Val moiety (Fig. 14).<sup>161</sup> This gelator showed a high tendency to aggregate in several organic solvents. Due to the presence of a flexible alkyl spacer and several H-bonding groups, intramolecular folding took place in the sol state (Fig. 14a), which was confirmed by CD spectroscopy. Typical of a helix, two negative bands at 217 and 205 nm and a positive lobe at *ca.* 187 nm were observed.

Two methods were used to prepare gels: (1) the solution containing the solid gelator was heated, and spontaneously cooled to 25 °C in a few minutes; (2) a slow, controlled cooling protocol was used for samples at concentrations close to or above 30 mM. CD spectroscopy was employed to investigate the different conformations of the gelator under these conditions. In the first method, dramatic changes in the shapes, positions and intensities of the bands were found upon increasing the concentration of the gelator from 0.6 mM to 30 mM (Fig. 14b), which was ascribed to the formation of a supramolecular gel at a concentration near to 30 mM. Notably, a red shift corresponding to the helical band was observed, indicating the occurrence of an unfolding process. In the second method, a similar phenomenon in CD spectra was observed when the temperature was above 40 °C. However, very significant differences were observed in the CD spectrum at 35 °C. A new band appeared at 210 nm and increased in intensity with time together with the formation of a gel (Fig. 14c), indicating that

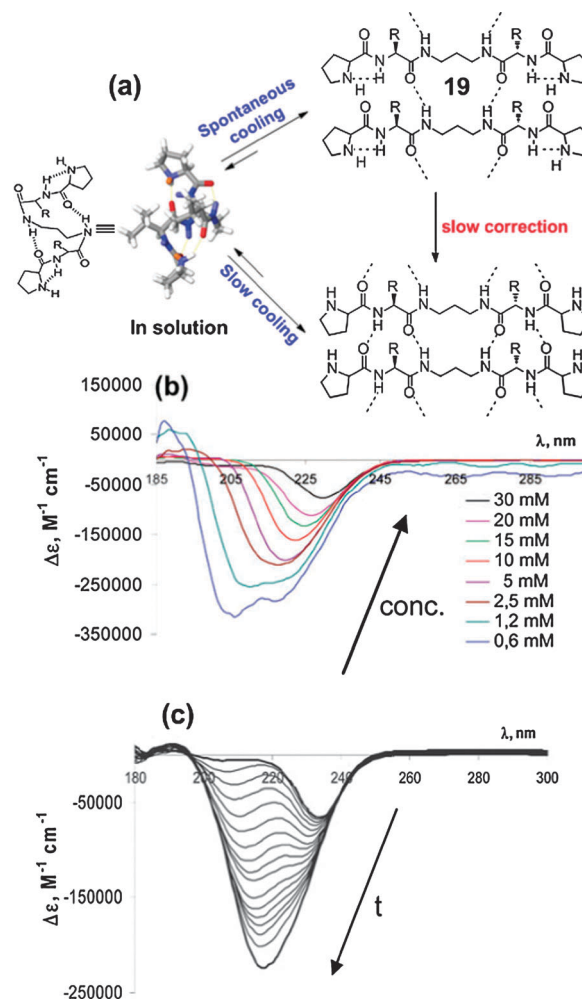


**Fig. 14** (a) The proposed packing modes in different states. (b) CD spectra of **19** at different concentrations in  $\text{CH}_3\text{CN}$  under spontaneous cooling. (c) Evolution of the CD spectrum of **19** (30 mM) in  $\text{CH}_3\text{CN}$  at 35 °C after slow cooling (5 min per step) (reproduced with permission of The Royal Society of Chemistry from ref. 161).

slow conformational changes took place. The reasons are: in the first method, the gelator molecules formed metastable aggregates, while for the molecular aggregation in the second method, slow and controlled cooling process allowed the evolution into aggregates with increased thermodynamic stability. The difference in these two methods resulted in the distinct sizes and aspects of the materials at the microscopic level, which was confirmed by SEM images.

## 6. Microscopy techniques

### 6.1 Scanning electron microscopy

Scanning electron microscopy (SEM) is a type of electron microscopy that produces images of a sample by scanning over it with a focused beam of electrons. These electrons interact with the electrons in the sample, producing various signals that can be detected and that contain information about the sample's surface topography and composition. The electron beam is generally scanned in a raster scan pattern, and the beam's position is combined with the detected signal to produce an image.

There are many advantages of using SEM in the supramolecular systems: (1) it is relatively cheap and widely available; (2) owing to the very narrow electron beam, it has a large depth of field, which allows a large area to be in focus at one time and yields a characteristic three-dimensional appearance; (3) SEM can produce images of very high resolution (several nanometers in size can be revealed); (4) a low magnification for the whole picture or a high magnification for the detailed structures of the samples can be easily achieved; (5) SEM three-dimensional images of the samples can be obtained due to its high depth of focus, which are very important.<sup>162</sup>

SEM is a versatile technique for supramolecular science and materials science to elucidate the microscopic structures of self-assembled systems owing to its high lateral resolution and great depth of focus. In most cases, SEM is used together with other microscopic techniques, such as atomic force microscope (AFM), transmission electron microscopy (TEM), and scanning tunneling microscopy (STM), which guarantees a complete understanding of the morphology of the sample.

Supramolecular gels can be regarded as a colloidal phase state in which a small amount of gelator immobilizes the bulk flow of a large amount of solvent molecules by the formation of 3D networks, which can consist of fibrillar structures. The fibers formed by self-assembly of molecular blocks with the size ranging from several nanometers to a few tens of micrometers. The size of these fibers are suitable for SEM, so SEM is an ideal method for observing their morphology.<sup>163–168</sup>

Rybchinski *et al.* reported a supramolecular gel based on perylene diimide (PDI) dye **20**, an extended aromatic system with interesting properties, such as multiple stimuli responsiveness, robustness, and advantageous light harvesting properties (Fig. 15).<sup>169</sup>

This gelator is an amphiphile with a hydrophobic core and two hydrophilic side chains. Due to the hydrophobically driven  $\pi$ - $\pi$  stacking interactions, it formed a supramolecular gel in

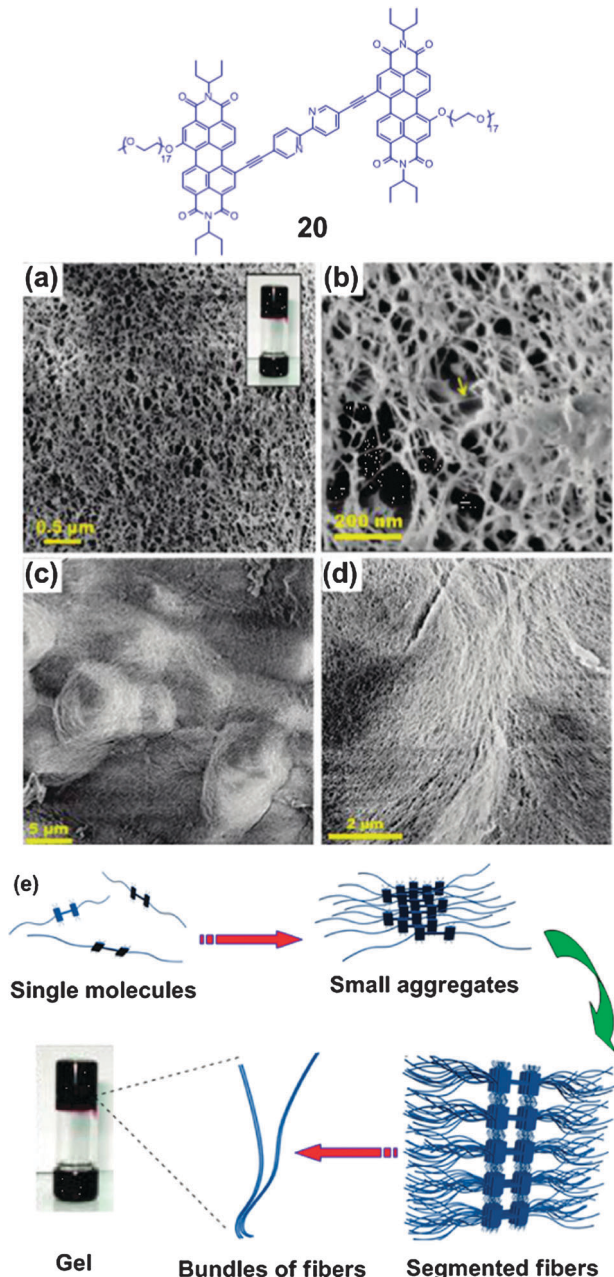


**Fig. 15** Cryo-SEM images of the gel ( $8 \times 10^{-3}$  M, a water-THF mixture with a volume ratio of 80:20) at different magnifications: (a) nanoporous structure of the three-dimensional networks (inset: vial inversion test); (b) image at high magnification; (c) whirls with diameters of 10–15  $\mu\text{m}$ ; (d) directional arrangement of fibers within a “microstream” in the gel. (e) Schematic illustration of **20** assembly hierarchy (reproduced with permission of American Chemical Society from ref. 169).

water-THF mixtures. Cryogenic scanning electron microscopy (cryo-SEM) revealed an interconnected porous structure of the gel, in which nanofibers form a 3D network. The average width of these fibers is  $6.1 \pm 1.1$  nm, while their actual average width is  $5.5 \pm 1.1$  nm, similar to the size observed in the case of the solution-phase network. Furthermore, thicker fibers with various diameters can be observed in the SEM images. The presence of whirls and streams several micrometers in size

demonstrated that the gel was composed of certain long-range order fibers. Based on these observations and other characteristic methods, the formation mechanism for the gelation process was depicted as shown in Fig. 15e. First, small aggregates containing 8–10 molecules were formed due to the hydrophobic effect and  $\pi$ - $\pi$  interactions. Due to the steric bulk of the aliphatic chains, the stacked molecules were shifted with respect to each other. Second, substantial hydrophobic domains were formed driven by the hydrophobic effect caused by the aliphatic side chains of PDI imide substituents, resulting in the formation of fibers with distinct segmentation. Then these fibers assembled into entangled bundles, which resulted in the formation of 3D networks.

## 6.2 Transmission electron microscopy

Transmission electron microscopy (TEM) is another microscopy technique whereby a beam of electrons interacts with the specimen as it passes through. An image can form from the interaction of the electrons with the specimen. The image is magnified and focused onto an imaging device, such as a fluorescent screen, or a layer of photographic film, or a sensor (CCD camera). In principle, TEM provides resolution high enough to observe molecules at the subnanometer scale.

TEM is currently used for the structural characterization of various supramolecular systems. For example, TEM has been actively employed to evaluate the thickness of lipid layers and their three-dimensional superstructures. As for the supramolecular assemblies of synthetic lipids, such as micelles, vesicles, tubes, and fibers, TEM imaging has been used as an essential tool to elucidate the morphology. TEM imaging has also been applied for the structural characterization of lipid hybrids with other supramolecular components, for example, peptides, nucleotides, carbon nanotubes, and inorganic components.

Notably, TEM has been widely employed for the structural characterization of supramolecular gels.<sup>170–175</sup> The superstructures self-assembled by gelators through multiple noncovalent interactions can be clearly observed by TEM. By analyzing the size and shape of the aggregates, important information can be obtained about the gelation process and mechanism.

Thixotropy plays a dramatically important role in the human body, for example, the functions of protoplasm, red blood cells, synovial fluid, and muscular activities are regulated by thixotropy. Despite the significant potential of this dynamic phenomenon, there is a lack of materials that can act as model systems to investigate vital natural processes such as muscle thixotropy and nerve fiber regeneration.<sup>175</sup> Shinkai *et al.* reported an interesting thixotropic gel based on naphthalene-diimide which can disintegrate in solution under an external mechanical stress and can regain its elastic properties upon removal of the stress (Fig. 16).<sup>176</sup>

In order to investigate how such self-assembled entities evolve under mechanical stress followed by a resting time, discernible visual insights into the processes are required. TEM was utilized to monitor these processes. Fig. 16a and b showed that the original gel based on **21** consists of 1D fibers several tens of micrometers in length and 10–150 nm in

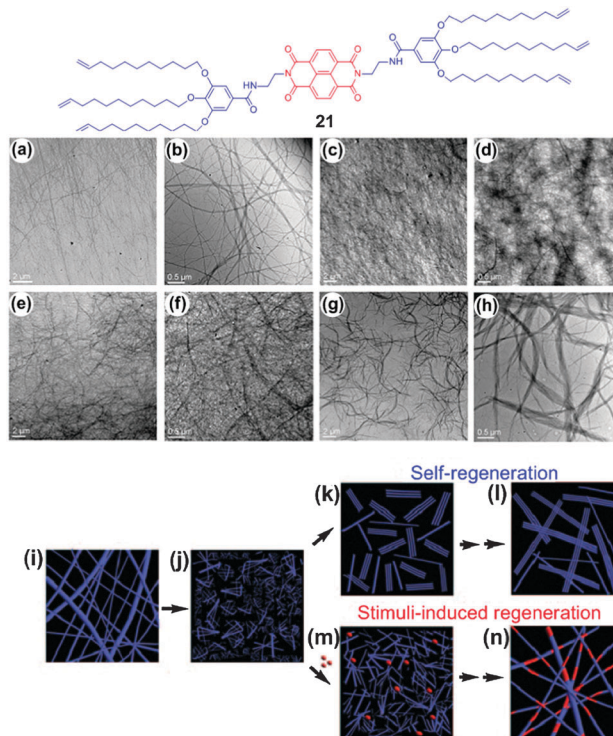


**Fig. 16** TEM images (at low and high magnifications): (a,b) original organogel **21** with extremely long (several tens of mm) fibers and large bundles with 10–100 nm in diameter; (c,d) images taken just after the disintegration of the gel (within 60 s) showing small fibers and clusters of many small fibers (black regions); (e,f) images taken after 6 h showing that the self-regeneration of the fibers and bundles have grown up to 5  $\mu$ m in length; (g,h) images after 40 h showing the regeneration of the fibers and bundles that have grown up to 10 mm in length. Schematic representation of the thixotropic process and its regulation with donor molecules: (i) original gel with long fibers; (j) short fibers after mixing by vortexing; (k,l) self-regeneration of fibers and bundles; (m,n) stimuli-induced regeneration of fibers in the presence of a molecular adhesive (red dots: 1,3-dihydroxynaphthalene) (reproduced with permission of John Wiley & Sons, Inc. from ref. 176).

diameter. The original long thin fibers and the thick bundles disintegrated into numerous small fibers after vortexing (Fig. 16b and c). As the solution underwent reconstitution and reverted back to the gel state after resting 24 hours, the fibers self-regenerated and the length of the bundles recovered to 8–10  $\mu$ m. The recovered gel is slightly weaker than the original gel because the reconstituted bundles are formed from loosely packed unimolecular fibers (Fig. 16h). Furthermore, the self-regeneration of these fibers took place even after vortexing for 48 hours at a concentration as low as 0.07 wt%, which was confirmed by AFM and TEM images. The donor molecules acted as molecular adhesives bringing the disintegrated active ends of the fibers together closely. This self-healing process monitored by TEM provided convincing evidence for its thixotropic behavior.

It should be noted that the morphologies observed in standard SEM and TEM are highly dependent on the method for sample preparation. Significant drying effects may cause considerable distortion of samples in the process of forming an xerogel, so the SEM (or TEM) observation can not always

provide the real morphologies of the aggregating structures. Cryo-SEM and cryo-TEM that are conducted in the freezing media can minimise morphological changes during sample drying as the gel is effectively 'frozen' in a rapid step inhibiting nanoscale reorganisation.<sup>177</sup> On the other hand, aging effects can lead to significant changes in the nanostructure of the gel as reported by Smith and coworkers.<sup>178</sup> Distinct nanoscale networks with twisted rope-like fibres were observed after allowing the gels to age for a period of time, assisting the chemists to know whether the gels were actually in their optimum thermodynamic state.

Conventional SEM requires samples to be imaged under vacuum, because a gas atmosphere rapidly spreads and attenuates electron beams. As a consequence, samples that produce a significant amount of vapour, such as wet biological samples or oil-bearing rock, must be either dried or cryogenically frozen. Environmental scanning electron microscope (ESEM) can be applied to study wet, fatty, or insulating materials without fixation, dehydration, or metal coating, under very low vacuum. Tang and coworkers employed field-emission ESEM to observe the details of gel-crystal transformation based on the *meta*-hydroxy pyridinium salt of 1,2,4,5-benzene tetracarboxylic acid at a molar ratio of 1:2.<sup>179</sup> The vapor pressures were kept constant at  $560 \pm 10$  Pa for hydrated samples and  $410 \pm 10$  Pa for dehydrated samples. An entangled fibrillar network full of water could be observed by ESEM after 1 h storage, showing a typical feature for ordinary gels. At a storage time of 12 h, fibers and crystals were observed simultaneously in the sample. When the storage time was prolonged to 36 h, only prismatic crystals existed. This phenomenon could be revealed more clearly for the dehydrated samples.

### 6.3 Atomic force microscopy

Atomic force microscope (AFM) is one of the foremost tools for imaging, measuring, and manipulating matters at the nanoscale. The information is gathered by "feeling" the surface with a very sensitive "spring-board"-like cantilever. Attractive or repulsive interactions that influence the tip at the end of cantilever as it is moved over a sample cause the cantilever to bend, thereby providing a mechanical means to probe local nanoscale effects.

AFM has many advantages for the study of supramolecules on surfaces: (1) high-resolution images ranging from nanometer to sub-millimeter length scales can be monitored; (2) AFM can provide a three-dimensional surface profile; (3) its applicability ranges from gaseous to liquid environments; (4) samples viewed by AFM do not require any special treatment (such as metal/carbon coating) that would irreversibly change or damage the samples, and typically do not suffer from charging artifacts in the final images; (5) it can be used to measure attractive interaction forces or energies of the supramolecular assemblies, for example, AFM-based single molecule force spectroscopy.<sup>180,181</sup> Notably, the key limitation of AFM is that the tip can lead to apparent flattening of soft matter nanostructures, making them appear wider and shallower than is actually the case.

The charge-transfer (CT) interactions or donor-acceptor interactions between  $\pi$ -systems are an important class of non-covalent interactions and have been greatly exploited in the design and synthesis of host-guest systems. CT complexes are formed by the weak associations of two molecules or molecular subgroups, one of which acts as an electron donor and the other as an electron acceptor.<sup>182-184</sup>

George and co-workers reported a supramolecular hydrogel formed through charge-transfer-induced alternate coassembly (Fig. 17).<sup>185</sup> A coronene tetracarboxylate tetrapotassium salt (CS) was selected as the aromatic donor molecule and a dodecyl functionalized methyl viologen derivative (DMV) was chosen as the electron acceptor counterpart.

AFM was utilized to obtain a better insight into the self-assembly of the DMV/CS charge-transfer complex into 1D nanofibers and further formation of a hydrogel. AFM analysis of the DMV/CS hydrogel showed the formation of an entangled

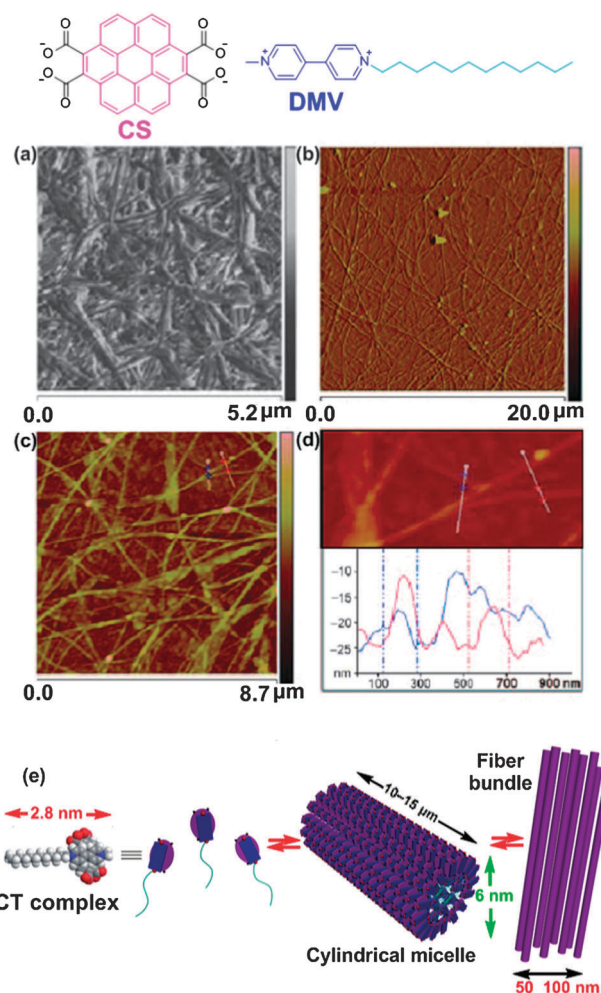


**Fig. 17** (a) Phase AFM image of the gel on a glass substrate. (b) AFM amplitude and (c) height images of the CS-DMV (1:1) complex on a glass substrate. (d) AFM height analysis of the isolated fibers; red and blue curves show the height profile of the fibers indicated by the lines in c and d. (e) Schematic representation of the hierarchical self-assembly of the CS-DMV CT amphiphile into cylindrical micelles and fiber bundles (reproduced with permission of John Wiley & Sons, Inc. from ref. 185).

network of very long fibers 10–15  $\mu\text{m}$  in length and 100–300 nm in diameter (Fig. 17a). Detailed AFM studies of 1:1 DMV–CS complex in water ( $1 \times 10^{-4}$  M) also confirmed a highly directional 1D self-assembly process, which was assisted by hydrophobic interactions of the supramolecular charge-transfer amphiphile along the  $\pi$ - $\pi$  stacking direction of the chromophore (Fig. 17b).

TEM analysis showed that the average diameter of the fibers was 6 nm, close to twice the length of the CT amphiphile, indicating a bilayer packing mode. The average height of the fibers was calculated to be 6–7 nm (Fig. 17c and d) by AFM, indicating that the CT amphiphiles formed by DMV and CS self-assembled into 1D cylindrical micelles in a radial fashion in the bilayer. The gelation process can be generalized as follows. First, CT amphiphiles formed between electron-poor DMV and electron-rich CS through charge-transfer interactions. Then, the CT amphiphiles self-assembled into high-aspect-ratio cylindrical micelles which gradually formed laterally associated fiber bundles through Coulombic interactions. Finally, the fibrous structures coil and entangle to form 3D networks, resulting in the formation of the hydrogel (Fig. 17e).

#### 6.4 Confocal laser scanning microscopy, polarized optical microscopy and fluorescence confocal microscopy

Confocal laser scanning microscopy (CLSM) is a technique for obtaining high-resolution optical images with depth selectivity.<sup>186</sup> The key feature of confocal microscopy is its ability to acquire in-focus images from selected depths, a process known as optical sectioning. Images are acquired point-by-point and reconstructed with a computer, allowing three-dimensional reconstructions of topologically complex objects. For opaque specimens, this is useful for surface profiling, while for non-opaque specimens, interior structures can be imaged. For interior imaging, the quality of the image is greatly enhanced over simple microscopy because image information from multiple depths in the specimen is not superimposed.<sup>187–189</sup> A conventional microscope “sees” as far into the specimen as the light can penetrate, while a confocal microscope only “sees” images one depth level at a time. In effect, the CLSM achieves a controlled and highly limited depth of focus.

Rowan and co-workers designed a versatile gelator containing the ligand 2,6-bis(1'-alkylbenzimidazolyl)pyridine (Fig. 18).<sup>190</sup> This bis-ligand functionalized compound **22** can be linked by Co(II) or Zn(II) ions to form a linear chain, because the ligand binds transition metal ions in a ratio of 2:1. However, for La(III) or Eu(III) ions, crosslinked networks can form because it can bind the larger lanthanide ions in a ratio of 3:1. These metallo-supramolecular polymer gels were shown to exhibit multiple stimuli-responsive behaviors, including thermo-, chemo-, and mechanical responses. One particularly interesting property of the metallo-induced supramolecular polymer gel is mechano-responsiveness, exhibiting a thixotropic (shear-thinning) behavior.

Laser scanning confocal microscopy was used to analyze the morphology of these phase-separated opaque gels, which

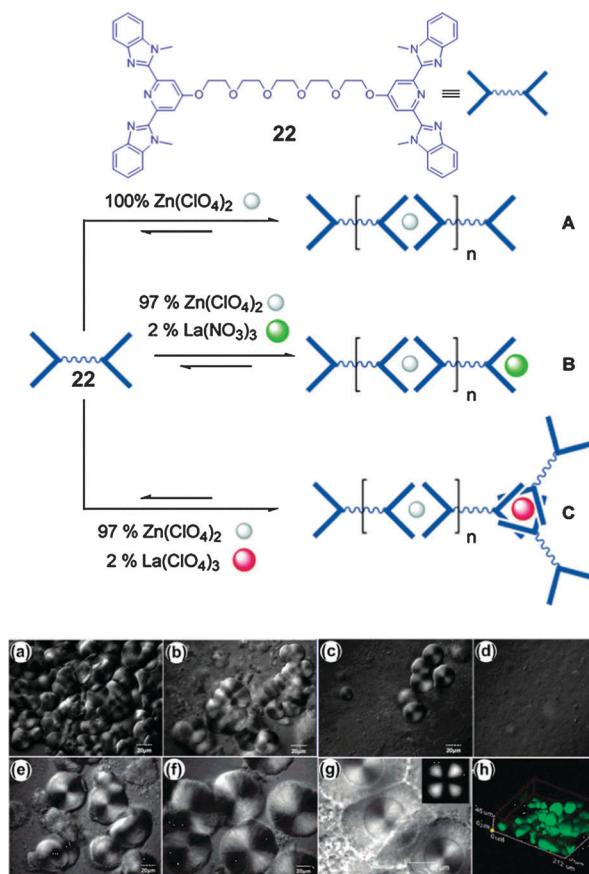


**Fig. 18** Top: representation of the metallo-supramolecular polymeric aggregates formed from the ditopic ligand end-capped monomer **22** with transition metal ions and/or lanthanide metal ions: (A),  $\text{Zn}(\text{ClO}_4)_2$ ; (B),  $\text{Zn}(\text{ClO}_4)_2$  and  $\text{La}(\text{NO}_3)_3$ ; (C),  $\text{Zn}(\text{ClO}_4)_2$  and  $\text{La}(\text{ClO}_4)_3$ . Middle: optical microscopic images showing the effect of mechanical history on the morphology of gel A (11 wt% in acetonitrile): (a) aircooled gel; (b) after shaking; (c) after shear at 50 Pa for 10 s; (d) after sonication for 2 min. Bottom: optical microscopic images of air-cooled gels (8 wt% in acetonitrile): (e) A,  $\text{Zn}(\text{ClO}_4)_2$  only; (f) B (mole ratio  $\text{Zn}(\text{ClO}_4)_2$ – $\text{La}(\text{NO}_3)_3 = 97/2$ ); (g) C (mole ratio  $\text{Zn}(\text{ClO}_4)_2$ – $\text{La}(\text{ClO}_4)_3 = 97/2$ ) obtained using a laser scanning confocal microscope operated in transmitted mode (the inset shows polarizing image of the gel C). (h) Laser scanning confocal microscopy (LSCM) showing 3D morphology of the globular structure in gel A (8 wt% in acetonitrile) (reproduced with permission of American Chemical Society from ref. 190).

provided insight into the gel formation mechanism. As shown in Fig. 18a, continuous globular particles with an average diameter around 20  $\mu\text{m}$  can be observed in the image for gel A (11 wt% in acetonitrile). The deformable globular particles are able to interpenetrate at the area of contact. The structure of the globular particles was destroyed significantly by the mechanical treatment. As shown in Fig. 18b, the number of the globular particles decreased dramatically when the gel was sheared at 50 Pa for just 10 s. All original globular particles disappeared when the sample was subjected to increasingly vigorous mechanical perturbation. The size of the resulting particles were closely related to the sonication energy and time applied to the sample, for example, the particles became smaller than 5  $\mu\text{m}$  in diameter under sonication for 2 min (Fig. 18d).

Microscopic examination provided evidence for the mechano-responsive property mentioned above. The broken fragments with smaller size caused by mechanical perturbation re-formed into an interconnecting network, which had denser and more homogeneous structures than were present in the fresh gels. These smaller particles in the re-formed gel increased surface area and generated more interparticle cross-linking sites in the networks, resulting in enhancement of the strength. Fluorescence confocal microscopy was also employed to investigate the morphology of the gel before and after mechanical perturbation. As shown in Fig. 18h, the density and the degree of particle interpenetration of the particles in less concentrated (8 wt%) samples are lower than those of the more concentrated gels (11 wt%).

The globular particles in the gels A, B, and C have different sizes and appearances. The diameter of the particles in gel A without lanthanum(III) ions varied from 20 to 40  $\mu\text{m}$  (Fig. 18e). For the particles in gel B containing 2 mol% lanthanum nitrate, the diameters were larger (30–60  $\mu\text{m}$ ) (Fig. 18f). Notably, the particles in gel C containing 2 mol% lanthanum perchlorate were the largest (as high as 100  $\mu\text{m}$ ) with a dense core (about 40  $\mu\text{m}$ ) and a large diffuse halo, indicating the presence of crystalline (or at least some ordered) structure (Fig. 18g). Confirmed by WAXS and morphological observations, crystallization of the supramolecular material accompanies gelation. For the particles in gels A and B, the diffuse halo was not so evident. The reason was that due to the formation of the internal branching networks, lanthanide cross-linkers made the cores of the globular entities crystalline or more highly ordered than the outer layer. Compared with noncoordinating perchlorate ion, the nitrate ion is coordinating in nature, so the branching was enhanced efficiently, resulting in the increase of the mechano-responsiveness of the gels.

## 7. Dynamic light scattering

Dynamic light scattering (DLS) is a technique especially useful in determining the size distribution profile, structural formation, and interactions of small particles in suspension, polymers in solution, or supramolecular systems. It can also be utilized to probe the behavior of complex fluids such as concentrated polymer solutions.

The mechanism of DLS is as follows: when a particle is subjected to Brownian motion and irradiated, two frequencies of equal intensity are generated in addition to the frequency that would normally be scattered, including a positive and negative Doppler shift proportional to the particle velocity. The interference between the nonshifted wave (proton re-emission) and the two waves due to Brownian motion yields infinitesimal variations in intensity. The scattered intensity is acquired as a function of time and is then self-correlated. This yields the relaxation time due to the Brownian motion and leads to the characterization of the particle size through hydrodynamic models of the diffusion coefficients.<sup>191</sup>

Periodic DLS measurements of a sample can provide information about how the particles aggregate over time. If particles

aggregate, there will be a larger population of particles with larger hydrodynamic radius. Additionally, stability depending on temperature can be analyzed by controlling the temperature *in situ*. Since DLS essentially measures fluctuations in scattered light intensity of the diffusing particles, the diffusion coefficient can also be determined. Studying the scattering of light by structures with sizes in the submicrometer range allows the determination of critical characteristics such as shape or internal structure. DLS is an efficient method in the characterization of supramolecular gels because the size (or the diffusion coefficient) changes dramatically upon the formation of 3D networks.

Jiang and co-workers reported an interesting photoresponsive polypseudorotaxane-type (PPR) hydrogel based on the competition of host-guest interactions (Fig. 19).<sup>192</sup> Linear polypseudorotaxane hydrogel formed in about 4 h by the self-assembly of poly(ethylene glycol) (PEG) as the axis and

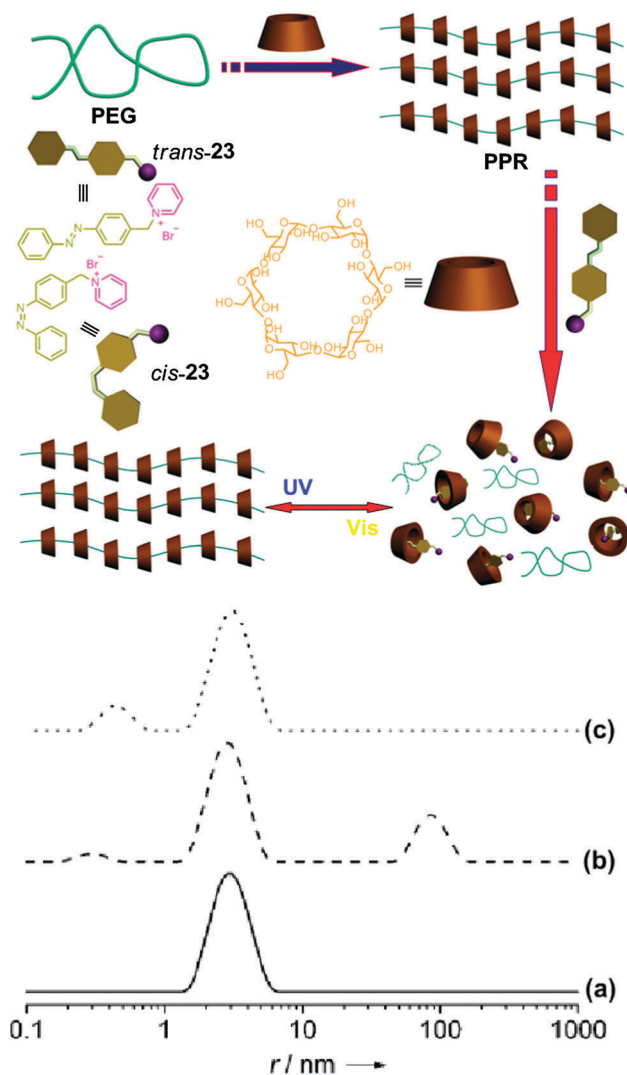


**Fig. 19** Cartoon representation of photoresponsive PPR gel-sol-gel transitions driven by competitive inclusion complexation. DLS results in aqueous solutions: (a) PEG; (b) PEG/ $\alpha$ -CD; (c) PEG/ $\alpha$ -CD/23 (reproduced with permission of John Wiley & Sons, Inc. from ref. 192).

$\alpha$ -cyclodextrins ( $\alpha$ -CDs) as wheels. 3D networks in this hydrogel arise from inclusion complexes between the PEG and CDs, where the threaded  $\alpha$ -CDs formed microcrystals acting as physical cross-linkers. The disassembly and reassembly of this hydrogel was realized by using a competitive guest 1-[*p*-(phenyl-azo)benzyl]pyridinium bromide (**23**) because the binding affinity between  $\alpha$ -CD and the azobenzene group is larger than that of  $\alpha$ -CD and PEG driven by hydrophobic interactions. This perfect work used the molecular recognition between *trans*-azobenzene and  $\alpha$ -CDs to achieve the deformation/re-formation of the hydrogel.

DLS was used to monitor the processes of the gel formation and dissociation. In order to prevent precipitation, DLS experiments were conducted in very dilute solutions (PEG at 0.01 g mL<sup>-1</sup>). As shown in Fig. 19 (curve a), a relatively narrow hydrodynamic radius distribution with a peak at 3 nm ascribed to PEG10K alone was observed. Upon addition of  $\alpha$ -CD, two new peaks appeared. The right-hand peak, with a size ranging from about 50 to 200 nm, was attributed to the formation of PEG/ $\alpha$ -CD linear complexes. The other peak with a size less than 1 nm is no doubt from the free  $\alpha$ -CD. Finally, the peak corresponding to the PPR aggregates completely disappeared when the guest **23** was added (Fig. 19c), which indicated that the PPR was dissociated by the formation of inclusion complexes between  $\alpha$ -CD and *tran*-**23**. The presence of a small peak located at less than 1 nm corresponded to the existence of small molecular complexes. Therefore, only free PEG chains and the inclusion complexes existed in this ternary system.

## 8. Thermal analysis

### 8.1 Isothermal titration calorimetry

Isothermal titration calorimetry (ITC) is a physical technique used to determine the thermodynamic parameters of interactions in solution. It is often used to study the noncovalent interactions among building blocks ranging from small molecules to macromolecules (such as proteins, DNA).

Noncovalent interactions in supramolecular chemistry involve exchanges of energy and momentum between the molecules. ITC offers the possibility to measure such an exchange, showing the immediate events taking place at the molecular level. ITC is a quantitative and ultrasensitive technique that can directly measure the binding affinity ( $K_a$ ), enthalpy changes ( $\Delta H$ ), and binding stoichiometry ( $n$ ) of the interaction between two or more molecules in solution. From these initial measurements, Gibbs energy changes ( $\Delta G$ ) and entropy changes ( $\Delta S$ ) can be determined using the relationship:

$$\Delta G = -RT \ln K_a = \Delta H - T\Delta S$$

Notably, ITC is also a destruction-free, label-free, and rapid (takes 1–3 h) instrumental method that requires less than micromolar amounts of the sample to learn about the thermodynamic parameters of reversible molecular associations. The accuracy and reliability of ITC makes it the gold standard in the characterization of intermolecular interactions in solution.<sup>193</sup>

Cucurbit[8]uril (CB[8]) is a macrocyclic host molecule with relatively large cavity size (479 Å<sup>3</sup>) to encapsulate an electron-deficient aromatic moiety such as methyl viologen (MV) and an electron-rich aromatic moiety such as 2-naphthol (Np) inside its cavity to form a stable dynamic 1:1:1 ternary complex as demonstrated by Kim and coworkers.<sup>194</sup> Scherman and co-workers elegantly utilized this CB[8]-based 1:1:1 ternary binding motif in water to construct a supramolecular polymeric hydrogel (Fig. 20).<sup>195</sup> Multivalent polymeric scaffolds with relatively low molecular weight ( $M_n < 40$  kDa) were prepared containing either electron-poor methyl viologen (**24**) or electron-rich naphthoxy derivatives (**25**). Upon addition of CB[8], the two multivalent copolymers bearing MV and Np guests, respectively, were connected by CB[8], resulting in the formation of a supramolecular hydrogel.

ITC was used to fully study the binding thermodynamic parameters of this supramolecular gel. The association constant between **24** and **25** was calculated to be  $8.0 (\pm 0.5) \times 10^4$  M<sup>-1</sup>. At the same time, other thermodynamic parameters ( $\Delta H$ ,  $\Delta S$ ,  $\Delta G$ ) were also obtained. Fig. 20b displays the ITC data for the titration of **25** into a buffered solution of **24**/CB[8]. It showed an isotherm that fits quite well to a one-set-of-sites binding model, indicating binding interactions between **25** and **24**/CB[8] in a 1:1 molar ratio. Additional investigations by ITC of polymer–polymer binding showed that the multivalent binding interactions were noncooperative, *i.e.* the strength of each binding interaction was independent of all others. These results indicated that the random and long-range spacing of

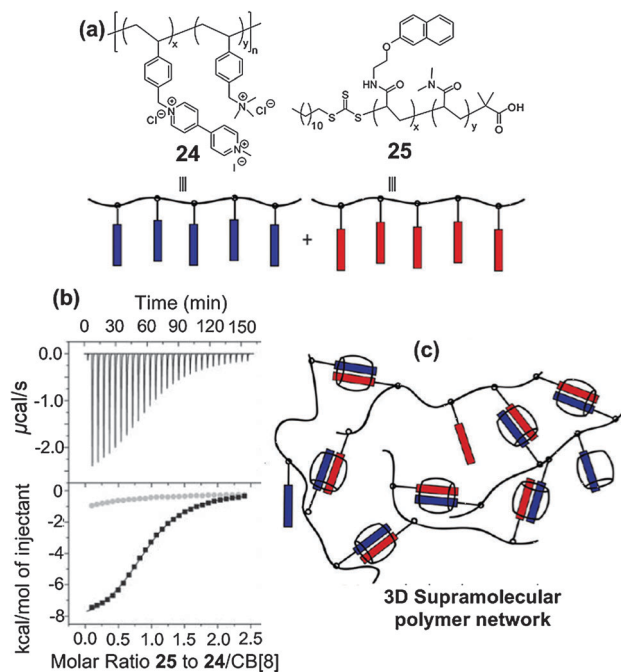


**Fig. 20** (a) Chemical structures of methyl viologen-functionalized polymer **24** and naphthoxy-functionalized polymer **25**. (b) ITC data for the binding of **25** to **24**/CB[8] at 25 °C in 10 mM PBS buffer at pH 7.0. (c) Cartoon representation of the formation of a 3D supramolecular network from **24** and **25** crosslinked by cucurbit[8]uril (reproduced with permission of American Chemical Society from ref. 195).

functional monomers along the polymer scaffold allowed the formation of large, cross-linked aggregates and networks.

## 8.2 Differential scanning calorimetry

Differential scanning calorimetry (DSC) is a thermoanalytic technique in which the difference in the amount of heat required to increase the temperature of a sample and the reference is measured as a function of temperature.<sup>196</sup>

The basic principle underlying this method is that when the sample undergoes a physical transformation, more or less heat will be needed for the sample than the reference to maintain both at the same temperature. Whether less or more heat must flow to the sample depends on whether the process is exothermic or endothermic. From a certain perspective, gelation is effectively a highly controlled crystallisation event driven by non-covalent interactions, with crystal growth only occurring in one dimension. An exothermic peak can be monitored when the gel undergoes a transition from gel to sol because it requires more heat flowing to the sample to increase its temperature at the same rate as the reference. On the contrary, less heat is required to raise the sample temperature as the sample undergoes exothermic processes as a sol-gel transition occurred.<sup>197</sup>

By observing the difference in heat flow between the sample and the reference, differential scanning calorimeters are able to measure the amount of heat absorbed or released during such transitions.<sup>198</sup> The result of a DSC experiment is a curve of heat flux *versus* temperature or *versus* time. The enthalpy of the gel-sol transition (or sol-gel transition) can be calculated from the DSC curve by integrating the peak corresponding to a given transition. In order to provide a more ordered sharp transition, the concentration of the sample is often relatively high, or the systems have a good degree of crystallinity.

Bhattacharya *et al.* reported two-component hydrogels by simply using fatty acids and amines.<sup>199</sup> The formation of such hydrogels depends on the hydrophobicity of the fatty acid as well as the type of amine used. Notably, stearic acid (**26**) is not soluble in water by itself, while it can form a gel with tetraethylenepentamine (**27**) on standing for 15–20 min at room temperature.

Differential scanning calorimetric studies were performed to gain further insights into the thermal stability of the gels. As shown in Fig. 21, when the gel was heated, a peak ascribed to the transition from gel to sol was observed. On the contrary, when the sol was cooled, a peak attributed to the transition from sol to gel was observed as well. Repeating the heating and cooling processes, similar transition peaks corresponding to the transitions from gel to sol and sol to gel were monitored, indicating the thermoreversible nature of the gel assembly. Importantly, the melting temperatures ( $T_m$ ) related to endothermic process when the gel changed into the sol state were found to be about 10–12 °C higher than the gel formation temperature ( $T_g$ ) corresponding to the exothermic process when the sol transformed into the gel state, which is typical of many LMWG-based gels.

From the DSC experiments, structure–property relationships between the acid and the amines were investigated.

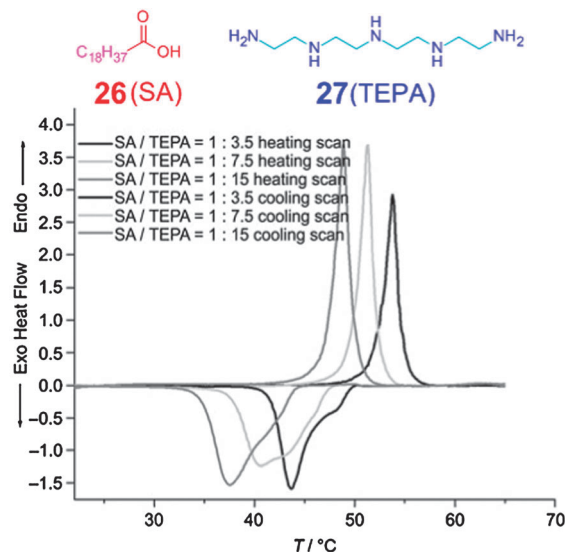


**Fig. 21** DSC thermograms of the gel of **26** (SA) and **27** (TEPA) at different molar ratios of acid and amine. The concentration of stearic acid in hydrogel is 0.07 M in each case (reproduced with permission of John Wiley & Sons, Inc. from ref. 199).

With increasing chain length in the diamine moieties from ethanediamine (EDA) to propanediamine (PDA) to butanediamine (BDA) to hexanediamine (HAD), thermal stabilities of the gel increased significantly. The reason was that the packing of the acid-amine salts in the gel became looser, resulting in the reduction of their stability. When the secondary amine proton was replaced by a methyl group, as in *N*-methyl-diethylenetriamine (MDTA) and *N*-methyl-imino-bis(propylamine) (MIBPA), the  $T_m$  values decreased drastically because the hydrogen bonds provided by secondary amino protons were abolished. Furthermore, the gels became slightly translucent and “loose”, reducing the  $T_m$  values as the concentration of the amine increased. The reason was that excess amines interferes with the hydrogen-bonded sites, which made it difficult to form 3D networks in the gel.

## 9. Rheology

Rheology or viscosimetry is the obvious choice when quantitative values are sought to describe the resistance to flow (the viscosity) of solutions or melts. Rheology can also yield useful information about the structures of the assemblies (their size or cross-linking density), about their dynamics, and even about their self-assembly mechanisms. For supramolecular gels, rheology is perhaps the most important defining feature.<sup>200–212</sup>

Steed *et al.* made a detailed and perfect introduction about the application of rheology in supramolecular gels.<sup>213</sup> Briefly speaking, rheology is the study of the deformation and flow of matter under the influence of an applied stress. When the sample is placed between two plates (or cylinders), upon applying a given oscillatory strain (or stress) to one of the plates, the induced movement of the other plate is decomposed into an in- and out-of-phase component. The elastic storage modulus ( $G'$ , the contribution of elastic) and elastic loss

modulus ( $G''$ , the contribution of viscous) can be measured as a function of applied stress or oscillation frequency.

Chemists always utilize two common rheological experiments to determine the formation of supramolecular gels: (1) the linear response of the modulus ( $G'$  and  $G''$ ) to a fixed small amplitude of stress by varying the frequency; (2) nonlinear behavior of the modulus to a fixed frequency by varying the shear stress. For typical supramolecular gels,  $G'$  should be invariant with frequency up to a yield stress corresponding to the transition from the gel state to the sol state and should exceed  $G''$  by at least an order of magnitude.<sup>214</sup>  $G'$  decreases rapidly above the yield stress, indicating the breakage of the networks. The behavior and magnitude of the moduli ( $G'$  and  $G''$ ) and yield stress as a function of applied stress (oscillatory frequency or concentration) can be modeled mathematically, and lead to conclusions about the structure of the gel.<sup>213</sup>

Aida and coworkers used electrostatic interactions between poly(sodium acrylate) (ASAP) treated clay nanosheets (CNS) and telechelic PEG polymers containing multivalent guanidinium dendritic endgroups of various generations (G1–G3) on both sides to prepare high-water content (96–98% water) hydrogels (Fig. 13).<sup>215</sup> Hydrogels with exceptional mechanical strength ( $G'$  up to  $10^6$  Pa) and rapid self-healing properties were formed rapidly upon mixing the cationic 'binder' and anionic silicate based clay nano-sheets through multivalent electrostatic interactions.

Rheological experiments were utilized to investigate the mechanical and self-healing properties of these hydrogels. As shown in Fig. 22a, The  $G'$  values were always larger than the  $G''$  values over the entire range of frequencies, typical of gels. Due to the multivalent effect, the G3-binder gave a hydrogel with the greatest  $G'$  value among these three binders.

From comparison of Fig. 22a and b, it was known that ASAP played a significant role in the mechanical strength of these supramolecular gels. The pretreatment of CNSs with ASAP caused the  $G'$  value to increase by a factor of up to six. On the other hand, the  $G'$  values were closely related to the amount of CNS (Fig. 22c) the  $G'$  values showed dramatic enhancement upon increasing the ratio of CNS.

The  $G'$  value of the gel containing 5.0% CNS, 0.38% G3 binder and 0.15% ASAP decreased rapidly above the critical strain region ( $\gamma = 59.0\%$ ), indicating a transition from the gel state to the sol state (Fig. 22e). Notably, convincing evidence about the excellent self-healing property of these gels was provided by rheological experiments. As shown in Fig. 12f, the  $G'$  value decreased from 0.5 MPa to 5 KPa upon application of a large amplitude oscillatory force ( $\gamma = 100\%$ ; frequency,  $\omega = 6.0 \text{ rad s}^{-1}$  (1.0 Hz)), resulting in a quasi-liquid state ( $\tan \delta \equiv G''/G' \approx 3.0\text{--}4.0$ ). On the contrary,  $G'$  immediately recovered its initial value and the system recovered to a quasi-solid state ( $\tan \delta \approx 0.4\text{--}0.5$ ) when the amplitude decreased ( $\gamma = 0.1\%$ ) at the same frequency (1.0 Hz).

The self-healing mentioned above is one of the most amazing properties in nature,<sup>216–218</sup> an ability of biological or artificial systems to spontaneously repair their damage and restore their original state. Different from most soft materials, which are not

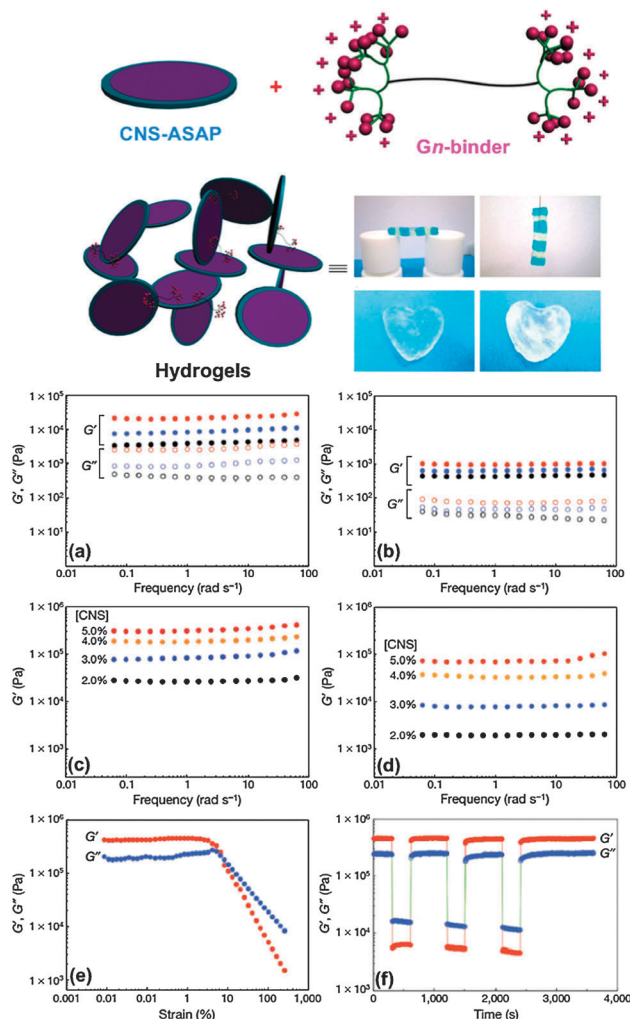


**Fig. 22** Top: cartoon representation of hydrogels formation. Bottom:  $G'$  and  $G''$  values of hydrogels (2.0% CNS,  $G_n$ -binder ( $n = 1$  (black),  $n = 2$  (blue),  $n = 3$  (red)), [guanidinium ion] = 0.5 mM): (a) with poly(sodium acrylate) (ASAP) (0.06%); (b) without ASAP. (c)  $G'$  values of hydrogels (2.0–5.0% CNS, CNS/G3-binder/ASAP = 1.0/0.075/0.03). (d)  $G'$  values of hydrogels (2.0–5.0% CNS, CNS/G3-binder/ASAP = 1.0/0.075/0).  $G'$  and  $G''$  values of a hydrogel (5.0% CNS, 0.38% G3-binder, 0.15% ASAP): (e) on strain sweep; (f) in continuous step strain measurements. Rheological properties of hydrogels were investigated at 20 °C. (reproduced with permission of Nature Publishing Group from ref. 215).

injectable, self-healing gels can regenerate the integral network after damage. This property endows these materials vast applications in the fields of drug delivery, 3D cell proliferation and tissue engineering.<sup>219–221</sup> Wei and coworkers constructed a hybrid magnetic self-healing hydrogel incorporating  $\text{Fe}_3\text{O}_4$  into hydrogel systems.<sup>222</sup> Rheological analyses provided definite evidence of the self-healing process.

The macroscopic properties of the supramolecular gels can be elucidated in a visual way using simple methods, such as tube inversion tests. Critical gelation concentration (CGC) and the gel–sol transition temperature ( $T_g$ ) can be measured utilizing this method. Additionally, the temperature of gelation can also be determined using “ball drop method”, in which a small glass ball is placed on the top of a gel while it is being heated.

However, the data obtained from these two methods are not so accurate. Some compounds without any gelation ability can also show gel-like phenomena when the concentrations are extremely high in a suitable solvent. On the other hand, the  $T_g$  values measured in small diameter tubes are always higher than those conducted in wider ones because the tubes with smaller diameter can enhance gelation. Similarly, the CGC values measured in tubes with smaller diameter are often lower than their real CGC values.<sup>178</sup>

## 10. Other methods

In addition to the commonly used methods mentioned above, other methods have also been used for the characterization of supramolecular gels. Zhang *et al.* innovatively utilized single molecule force spectroscopy (SMFS), a developing technique based on AFM, to study the supramolecular polymerization driven by multiple host-stabilized charge-transfer interactions.<sup>223,224</sup> Ajayaghosh and coworkers used single-wall carbon nanotube (SWNT) triggered self-assembly of oligo(*p*-phenylene vinylene)s (OPVs) to stabilize hybrid  $\pi$ -gels. Thermogravimetric analysis (TGA) revealed the pyrolysis temperature and the composition of the OPV-SWNT composite gel.<sup>225</sup> MacLachlan and coworkers utilized electrospray ionization mass spectrometry (ESI-MS) to get a snapshot of large aggregates of zinc salphen complexes in solution, which provided evidence for the formation of metal-containing gel.<sup>226</sup> Similarly, MALDI-TOF-MS is another especially useful method for the detection of organo-metallic gelators.<sup>227–229</sup> Accompanied by the formation of gels, the turbidity of the solution always changes significantly. Therefore, turbidity experiments is another efficient method to confirm the formation of gels.<sup>230–234</sup>

## 11. Conclusions and outlook

Supramolecular gels are a fantastic class of soft and responsive soft materials, and the amount of research devoted to these fascinating supra-macromolecules is rapidly increasing due to their wide applications ranging from sensors to biomaterials. Undoubtedly, the better the gelation mechanism and properties of supramolecular gels are understood, the more innovatively these promising materials can be developed. However, it is difficult for chemists to fully characterize these novel materials due to their dynamic nature. Here we discussed various methods for the characterization of supramolecular gels. For the full investigation of supramolecular gels, suitable methods should be carefully chosen according to the distinct gelation mechanisms and influencing factors of supramolecular gels, because every characterization method has its own advantages and disadvantages. More importantly, multiple experimental techniques should be combined cooperatively to obtain convincing conclusions. In order to make better use of the supramolecular gels and bring benefits for human beings, more efforts need to be made by scientists to develop new and more efficient characterization methods for supramolecular gels.

We believe that the tomorrow of supramolecular gels will definitely be bright.

## Acknowledgements

Feihe Huang is very grateful to Professor Harry W. Gibson for his enormous support and encouragement. National Basic Research Program (2013CB834502), the National Natural Science Foundation of China (91027006 and 21125417), the Fundamental Research Funds for the Central Universities (2012QNA3013), and Open Project of State Key Laboratory of Supramolecular Structure and Materials are greatly acknowledged for their generous financial support.

## References

- 1 H. Maeda, *Chem.–Eur. J.*, 2008, **14**, 11274.
- 2 G. O. Lloyd and J. W. Steed, *Nat. Chem.*, 2009, **1**, 437.
- 3 S. Banerjee, R. K. Das and U. Maitra, *J. Mater. Chem.*, 2009, **19**, 6649.
- 4 J. W. Steed, *Chem. Soc. Rev.*, 2010, **39**, 3686.
- 5 P. Terech and R. G. Weiss, *Chem. Rev.*, 1997, **97**, 3133.
- 6 L. A. Estroff and A. D. Hamilton, *Chem. Rev.*, 2004, **104**, 1201.
- 7 P. J. Flory, *Faraday Discuss. Chem. Soc.*, 1974, **57**, 7.
- 8 A. Noro, M. Hayashi and Y. Matsushita, *Soft Matter*, 2012, **8**, 6416.
- 9 S. Seiffert and J. Sprakel, *Chem. Soc. Rev.*, 2012, **41**, 909.
- 10 J. A. Foster and J. W. Steed, *Angew. Chem., Int. Ed.*, 2010, **49**, 6718.
- 11 J. W. Steed, *Chem. Commun.*, 2011, **47**, 1379.
- 12 E. A. Appel, J. Barrio, X. J. Loh and O. A. Scherman, *Chem. Soc. Rev.*, 2012, **41**, 6195.
- 13 L. E. Buerkle and S. J. Rowan, *Chem. Soc. Rev.*, 2012, **41**, 6089.
- 14 S. K. Samanta, A. Pal, S. Bhattacharya and C. N. R. Rao, *J. Mater. Chem.*, 2010, **20**, 6881.
- 15 X. Yan, F. Wang, B. Zheng and F. Huang, *Chem. Soc. Rev.*, 2012, **41**, 6042.
- 16 S. Dong, X. Yan, B. Zheng, J. Chen, X. Ding, Y. Yu, D. Xu, M. Zhang and F. Huang, *Chem.–Eur. J.*, 2012, **18**, 4195.
- 17 D. J. Abdallah, S. A. Sirchio and R. G. Weiss, *Langmuir*, 2000, **16**, 7558.
- 18 L. E. Echegoyen, L. Portugal, S. R. Miller, J. C. Hernandez, L. Echegoyen and G. W. Gokel, *Tetrahedron Lett.*, 1988, **29**, 4065.
- 19 A. R. Hirst, D. K. Smith and J. P. Harrington, *Chem.–Eur. J.*, 2005, **11**, 6552.
- 20 Y. Zhou, T. Yi, T. Li, Z. Zhou, F. Li, W. Huang and C. Huang, *Chem. Mater.*, 2006, **18**, 2974.
- 21 J. H. Jung, Y. Ono, K. Sakurai, M. Sano and S. Shinkai, *J. Am. Chem. Soc.*, 2000, **122**, 8648.
- 22 C. B. Minkenberg, W. E. Hendriksen, F. Li, E. Mendes, R. Eelkema and J. H. van Esch, *Chem. Commun.*, 2012, **48**, 9837.

- 23 A. Harada, R. Kobayashi, Y. Takashima, A. Hashidzume and H. Yamaguchi, *Nat. Chem.*, 2011, **3**, 34.
- 24 T. Park and S. C. Zimmerman, *J. Am. Chem. Soc.*, 2006, **128**, 11582.
- 25 M. Shirakawa, N. Fujita and S. Shinkai, *J. Am. Chem. Soc.*, 2003, **125**, 9902.
- 26 J. R. Moffat, G. J. Seeley, J. T. Carter, A. Burgessb and D. K. Smith, *Chem. Commun.*, 2008, 4601.
- 27 E. Carretti, M. Bonini, L. Dei, B. H. Berrie, L. V. Angelova, P. Baglioni and R. G. Weiss, *Acc. Chem. Res.*, 2010, **43**, 751.
- 28 S. R. Haines and R. G. Harrison, *Chem. Commun.*, 2002, 2846.
- 29 K. Tsuchiya, Y. Orihara, Y. Kondo, N. Yoshino, T. Ohkubo, H. Sakai and M. Abe, *J. Am. Chem. Soc.*, 2004, **126**, 12282.
- 30 T. Ogoshi, Y. Takashima, H. Yamaguchi and A. Harada, *J. Am. Chem. Soc.*, 2007, **129**, 4878.
- 31 Y. Kohsaka, Y. Koyama and T. Takata, *Angew. Chem., Int. Ed.*, 2011, **50**, 10417.
- 32 A. R. Hirst, B. Escuder, J. F. Miravet and D. K. Smith, *Angew. Chem., Int. Ed.*, 2008, **47**, 8002.
- 33 J. A. Foster, M.-O. M. Piepenbrock, G. O. Lloyd, N. Clarke, J. A. K. Howard and J. W. Steed, *Nat. Chem.*, 2010, **2**, 1037.
- 34 N. M. Sangeetha and U. Maitra, *Chem. Soc. Rev.*, 2005, **34**, 821.
- 35 Z. Yang, G. Liang and B. Xu, *Acc. Chem. Res.*, 2008, **41**, 315.
- 36 Z. Ge, J. Hu, F. Huang and S. Liu, *Angew. Chem., Int. Ed.*, 2009, **48**, 1798.
- 37 C. Deng, R. Fang, Y. Guan, J. Jiang, C. Lin and L. Wang, *Chem. Commun.*, 2012, **48**, 7973.
- 38 Q. Liu, Y. Wang, W. Li and L. Wu, *Langmuir*, 2007, **23**, 8217.
- 39 J.-W. Liu, Y. Yang, C.-F. Chen and J.-T. Ma, *Langmuir*, 2010, **26**, 9040.
- 40 R. N. Das, Y. P. Kumar, S. Pagoti, A. J. Patil and J. Dash, *Chem.-Eur. J.*, 2012, **18**, 6008.
- 41 F. Huang, K. A. Switek, L. N. Zakharov, F. R. Fronczek, C. Slebodnick, M. Lam, J. A. Golen, W. S. Bryant, P. E. Mason, A. L. Rheingold, M. Ashraf-Khorassani and H. W. Gibson, *J. Org. Chem.*, 2005, **70**, 3231.
- 42 J. Liu, P. He, J. Yan, X. Fang, J. Peng, K. Liu and Y. Fang, *Adv. Mater.*, 2008, **20**, 2508.
- 43 S. Dong, B. Zheng, D. Xu, X. Yan, M. Zhang and F. Huang, *Adv. Mater.*, 2012, **24**, 3191.
- 44 X. Yan, D. Xu, X. Chi, J. Chen, S. Dong, X. Ding, Y. Yu and F. Huang, *Adv. Mater.*, 2012, **24**, 362.
- 45 B. Escuder, M. Llusar and J. F. Miravet, *J. Org. Chem.*, 2006, **71**, 7747.
- 46 A. R. Hirst, I. A. Coates, T. R. Boucheteau, J. F. Miravet, B. Escuder, V. Castelletto, I. W. Hamley and D. K. Smith, *J. Am. Chem. Soc.*, 2008, **130**, 9113.
- 47 A. R. Hirst, J. F. Miravet, B. Escuder, L. Noirez, V. Castelletto, I. W. Hamley and D. K. Smith, *Chem.-Eur. J.*, 2009, **15**, 372.
- 48 J. C. Martins, F. A. G. Mercier, A. Vandervelden, M. Biesemans, J.-M. Wieruszkeski, E. Humpfer, R. Willem and G. Lippens, *Chem.-Eur. J.*, 2002, **8**, 3431.
- 49 W. S. Price, *Concepts Magn. Reson.*, 1998, **10**, 197.
- 50 S. Iqbal, F. R. Llansola, B. Escuder, J. F. Miravet, I. Verbruggen and R. Willem, *Soft Matter*, 2010, **6**, 1875.
- 51 T. Xiao, X. Feng, S. Ye, Y. Guan, S. Li, Q. Wang, Y. Ji, D. Zhu, X. Hu, C. Lin, Y. Pan and L. Wang, *Macromolecules*, 2012, **45**, 9585.
- 52 T. Xiao, S. Li, Y. Zhang, C. Lin, B. Hu, X. Guan, Y. Yu, J. Jiang and L. Wang, *Chem. Sci.*, 2012, **3**, 1417.
- 53 Z. Zhang, Y. Luo, J. Chen, S. Dong, Y. Yu, Z. Ma and F. Huang, *Angew. Chem., Int. Ed.*, 2011, **50**, 1397.
- 54 A. Macchioni, G. Ciancaleoni, C. Zuccaccia and D. Zuccaccia, *Supramolecular Chemistry: From Molecules to Nanomaterials*, Wiley-VCH, 2012.
- 55 S. Dong, Y. Luo, X. Yan, B. Zheng, X. Ding, Y. Yu, Z. Ma, Q. Zhao and F. Huang, *Angew. Chem., Int. Ed.*, 2011, **50**, 1905.
- 56 F. Wang, C. Han, C. He, Q. Zhou, J. Zhang, C. Wang, N. Li and F. Huang, *J. Am. Chem. Soc.*, 2008, **130**, 11254.
- 57 F. Wang, J. Zhang, X. Ding, S. Dong, M. Liu, B. Zheng, S. Li, L. Wu, Y. Yu, H. W. Gibson and F. Huang, *Angew. Chem., Int. Ed.*, 2010, **49**, 1090.
- 58 W. Jiang, K. Nowosinski, N. L. Low, E. V. Dzyuba, F. Klautzsch, A. Schafer, J. Huuskonen, K. Rissanen and C. A. Schalley, *J. Am. Chem. Soc.*, 2012, **134**, 1860.
- 59 W. Jiang, A. Schäfer, P. C. Mohr and C. A. Schalley, *J. Am. Chem. Soc.*, 2010, **132**, 2309.
- 60 S. J. Loeb, J. Tiburcio and S. J. Vella, *Org. Lett.*, 2005, **7**, 4923.
- 61 K. Zhu, V. N. Vukotic and S. J. Loeb, *Angew. Chem., Int. Ed.*, 2012, **51**, 2168.
- 62 S.-H. Chiu, S. J. Rowan, S. J. Cantrill, P. T. Glink, R. L. Garrell and J. F. Stoddart, *Org. Lett.*, 2000, **2**, 3631.
- 63 A. M. Elizarov, S.-H. Chiu and J. F. Stoddart, *J. Org. Chem.*, 2002, **67**, 9175.
- 64 J. D. Badjić, S. J. Cantrill and J. F. Stoddart, *J. Am. Chem. Soc.*, 2004, **126**, 2288.
- 65 S.-Y. Hsue, C.-T. Kuo, T.-W. Lu, C.-C. Lai, Y.-H. Liu, H.-F. Hsu, S. M. Peng, C. Chen and S.-H. Chiu, *Angew. Chem., Int. Ed.*, 2010, **49**, 9170.
- 66 G. Yu, M. Xue, Z. Zhang, J. Li, C. Han and F. Huang, *J. Am. Chem. Soc.*, 2012, **134**, 13248.
- 67 K.-R. Wang, D.-S. Guo, B.-P. Jiang, Z.-H. Sun and Y. Liu, *J. Phys. Chem. B*, 2010, **114**, 101.
- 68 C. Li, K. Han, J. Li, H. Zhang, J. Ma, X. Shu, Z. Chen, L. Weng and X. Jia, *Org. Lett.*, 2012, **14**, 42.
- 69 S. Tamesue, Y. Takashima, H. Yamaguchi, S. Shinkai and A. Harada, *Angew. Chem., Int. Ed.*, 2010, **49**, 7461.
- 70 G. Yu, C. Han, Z. Zhang, J. Chen, X. Yan, B. Zheng, S. Liu and F. Huang, *J. Am. Chem. Soc.*, 2012, **134**, 8711.
- 71 D.-H. Qu, Q.-C. Wang, J. Ren and H. Tian, *Org. Lett.*, 2004, **6**, 4.
- 72 D.-H. Qu, Q.-C. Wang and H. Tian, *Angew. Chem., Int. Ed.*, 2005, **44**, 5296.
- 73 D.-H. Qu, Q.-C. Wang, X. Ma and H. Tian, *Chem.-Eur. J.*, 2005, **11**, 5929.
- 74 L. Zhu, X. Ma, F. Ji, Q. Wang and H. Tian, *Chem.-Eur. J.*, 2007, **13**, 9216.

- 75 V. Lozano, R. Hernández, A. Ardá, J. Jiménez-Barbero, C. Mijangos and M.-J. Pérez-Pérez, *J. Mater. Chem.*, 2011, **21**, 8862.
- 76 J. Keeler, *Understanding NMR Spectroscopy*, Wiley-VCH, 2010.
- 77 Y. Liu, D.-S. Guo, H.-Y. Zhang, F. Ding, K. Chen and H.-B. Song, *Chem.-Eur. J.*, 2007, **13**, 466.
- 78 C. Li, X. Shu, J. Li, S. Chen, K. Han, M. Xu, B. Hu, Y. Yu and X. Jia, *J. Org. Chem.*, 2011, **76**, 8458.
- 79 W. Deng, H. Yamaguchi, Y. Takashima and A. Harada, *Angew. Chem., Int. Ed.*, 2007, **46**, 5144.
- 80 K. Hamasaki, H. Ikeda, A. Nakamura, A. Ueno, F. Toda, I. Suzuki and T. Osa, *J. Am. Chem. Soc.*, 1993, **115**, 5035.
- 81 R. Sheehan and P. J. Cragg, *Supramolecular Chemistry: From Molecules to Nanomaterials*, Wiley-VCH, 2012.
- 82 J. A. Sáez, B. Escuder and J. F. Miravet, *Chem. Commun.*, 2010, **46**, 7996.
- 83 C. Dou, C. Wang, H. Zhang, H. Gao and Y. Wang, *Chem.-Eur. J.*, 2010, **16**, 10744.
- 84 A. Das, M. R. Molla, B. Maity, D. Koley and S. Ghosh, *Chem.-Eur. J.*, 2012, **18**, 9849.
- 85 S. V. Bhosale, C. H. Janiab and S. J. Langford, *Chem. Soc. Rev.*, 2008, **37**, 331.
- 86 T. Tu, X. Bao, W. Assenmacher, H. Peterlik, J. Daniels and K. H. Dötz, *Chem.-Eur. J.*, 2009, **15**, 1853.
- 87 S. J. George, A. Ajayaghosh, P. Jonkheijm, A. P. H. J. Schenning and E. W. Meijer, *Angew. Chem., Int. Ed.*, 2004, **43**, 3422.
- 88 A. Dawn, T. Shiraki, S. Haraguchi, H. Sato, K. Sada and S. Shinkai, *Chem.-Eur. J.*, 2010, **16**, 3676.
- 89 M. Tanaka, T. Ikeda, J. Mack, N. Kobayashi and T. Haino, *J. Org. Chem.*, 2011, **76**, 5082.
- 90 A. Aggeli, I. A. Nyrkova, M. Bell, R. Harding, L. Carrick, T. C. B. McLeish, A. N. Semenov and N. Boden, *Proc. Natl. Acad. Sci. U. S. A.*, 2001, **98**, 11857.
- 91 Y. S. Velichko, S. I. Stupp and M. O. de la Cruz, *J. Phys. Chem. B*, 2008, **112**, 2326.
- 92 S.-L. Li, T. Xiao, B. Hu, Y. Zhang, F. Zhao, Y. Ji, Y. Yu, C. Lin and L. Wang, *Chem. Commun.*, 2011, **47**, 10755.
- 93 G. D. Enright, S. Takeya and J. A. Ripmeester, *Supramolecular Chemistry: From Molecules to Nanomaterials*, Wiley-VCH, 2012.
- 94 Y.-S. Su, J.-W. Liu, Y. Jiang and C.-F. Chen, *Chem.-Eur. J.*, 2011, **17**, 2435.
- 95 C. Ren, S. Xu, J. Xu, H. Chen and H. Zeng, *Org. Lett.*, 2011, **13**, 3840.
- 96 T. Nakagaki, A. Harano, Y. Fuchigami, E. Tanaka, S. Kidoaki, T. Okuda, T. Iwanaga, K. Goto and T. Shinmyozu, *Angew. Chem., Int. Ed.*, 2010, **49**, 9676.
- 97 I. Hwang, W. S. Jeon, H. J. Kim, D. Kim, H. Kim, N. Selvapalam, N. Fujita, S. Shinkai and K. Kim, *Angew. Chem., Int. Ed.*, 2007, **46**, 210.
- 98 S. Doniach, *Chem. Rev.*, 2001, **101**, 1763.
- 99 M. Sutton, *C. R. Phys.*, 2008, **9**, 657.
- 100 A. R. Hirst, D. K. Smith, M. C. Feiters and H. P. M. Geurts, *Chem.-Eur. J.*, 2004, **10**, 5901.
- 101 C. A. Dreiss, T. Cosgrove, F. N. Newby and E. Sabadini, *Langmuir*, 2004, **20**, 9124.
- 102 B. Huang, A. R. Hirst, D. K. Smith, V. Castelletto and I. W. Hamley, *J. Am. Chem. Soc.*, 2005, **127**, 7130.
- 103 A. C. Toma and T. Pfohl, *Supramolecular Chemistry: From Molecules to Nanomaterials*, Wiley-VCH, 2012.
- 104 T. Park, S. C. Zimmerman and S. Nakashima, *J. Am. Chem. Soc.*, 2005, **127**, 6520.
- 105 W. Zhu, Y. Li, L. Liu, Y. Chen, C. Wang and F. Xi, *Biomacromolecules*, 2010, **11**, 3086.
- 106 N. Yan, G. He, H. Zhang, L. Ding and Y. Fang, *Langmuir*, 2010, **26**, 5909.
- 107 J. H. Jung, G. John, M. Masuda, K. Yoshida, S. Shinkai and T. Shimizu, *Langmuir*, 2001, **17**, 7229.
- 108 M. George and R. G. Weiss, *J. Am. Chem. Soc.*, 2001, **123**, 10393.
- 109 T. Park and S. C. Zimmerman, *J. Am. Chem. Soc.*, 2006, **128**, 13986.
- 110 M. Loos, J. Esch, R. M. Kellogg and B. L. Feringa, *Angew. Chem., Int. Ed.*, 2001, **40**, 613.
- 111 C. Wang, D. Zhang and D. Zhu, *J. Am. Chem. Soc.*, 2005, **127**, 16372.
- 112 C. Wang, D. Zhang, J. Xiang and D. Zhu, *Langmuir*, 2007, **23**, 9195.
- 113 C. Wang, D. Zhang and D. Zhu, *Langmuir*, 2007, **23**, 1478.
- 114 F. Rodríguez-Llansola, D. Hermida-Merino, B. Nieto-Ortega, F. J. Ramírez, J. T. L. Navarrete, J. Casado, I. W. Hamley, B. Escuder, W. Hayes and J. F. Miravet, *Chem.-Eur. J.*, 2012, **18**, 14725.
- 115 B. Jacrot, *Rep. Prog. Phys.*, 1976, **39**, 911.
- 116 S. J. Perkins, *Biochem. J.*, 1998, **254**, 313.
- 117 A. Walcarius, *Chem. Mater.*, 2001, **13**, 3351.
- 118 S. Tamaru, M. Takeuchi, M. Sano and S. Shinkai, *Angew. Chem., Int. Ed.*, 2002, **41**, 853.
- 119 J. Liu, G. Chen, M. Guo and M. Jiang, *Macromolecules*, 2010, **43**, 8086.
- 120 Y. Tian, L. Zhang, P. Duan, F. Liu, B. Zhang, C. Liu and M. Liu, *New J. Chem.*, 2010, **34**, 2847.
- 121 M. George, G. P. Funkhouser, P. Terech and R. G. Weiss, *Langmuir*, 2006, **22**, 7885.
- 122 N. Demirdöven, C. M. Cheatum, H. S. Chung, M. Khalil, J. Knoester and A. Tokmakoff, *J. Am. Chem. Soc.*, 2004, **126**, 7981.
- 123 M. Suzuki, M. Yumoto, H. Shirai and K. Hanabusa, *Chem.-Eur. J.*, 2008, **14**, 2133.
- 124 M. Yang, Z. Zhang, F. Yuan, W. Wang, S. Hess, K. Lienkamp, I. Lieberwirth and G. Wegner, *Chem.-Eur. J.*, 2008, **14**, 3330.
- 125 V. J. Nebot, J. Armengol, J. Smets, S. F. Prieto, B. Escuder and J. F. Miravet, *Chem.-Eur. J.*, 2012, **18**, 4063.
- 126 P. Misra and M. A. Dubinskii, *Ultraviolet Spectroscopy and UV Lasers*, Marcel Dekker, New York, 2002.
- 127 C. A. Strassert, C.-H. Chien, M. D. GalvezLopez, D. Kourkoulos, D. Hertel, K. Meerholz and L. D. Cola, *Angew. Chem., Int. Ed.*, 2011, **50**, 946.
- 128 T. Taira, Y. Suzuki and K. Osakada, *Chem.-Eur. J.*, 2010, **16**, 6518.

- 129 Y. Ogawa, C. Yoshiyama and T. Kitaoka, *Langmuir*, 2012, **28**, 4404.
- 130 T. Sugimoto, T. Suzuki, S. Shinkai and K. Sada, *J. Am. Chem. Soc.*, 2007, **129**, 270.
- 131 S. Bhattacharya and S. K. Samanta, *Chem.–Eur. J.*, 2012, **18**, 16632.
- 132 O. Kotova, R. Daly, C. M. G. Santos, M. Boese, P. E. Kruger, J. J. Boland and T. Gunnlaugsson, *Angew. Chem., Int. Ed.*, 2012, **51**, 7208.
- 133 H. Maeda and Y. Terashima, *Chem. Commun.*, 2011, **47**, 10344.
- 134 A. Hahma, S. Bhat, K. Leivo, J. Linnanto, M. Lahtinen and K. Rissanen, *New J. Chem.*, 2008, **32**, 1438.
- 135 I. Hisaki, H. Shigemitsu, Y. Sakamoto, Y. Hasegawa, Y. Okajima, K. Nakano, N. Tohnai and M. Miyata, *Angew. Chem., Int. Ed.*, 2009, **48**, 5465.
- 136 C. Wang, Q. Chen, F. Sun, D. Zhang, G. Zhang, Y. Huang, R. Zhao and D. Zhu, *J. Am. Chem. Soc.*, 2010, **132**, 3092.
- 137 J. T. Vivian and P. R. Callis, *Biophys. J.*, 2001, **80**, 2093.
- 138 K. V. Rao, K. K. R. Datta, M. Eswaramoorthy and S. J. George, *Angew. Chem., Int. Ed.*, 2011, **50**, 1179.
- 139 H.-J. Kim, J.-H. Lee and M. Lee, *Angew. Chem., Int. Ed.*, 2005, **44**, 5810.
- 140 Y. Zheng, A. Hashidzume, Y. Takashima, H. Yamaguchi and A. Harada, *Langmuir*, 2011, **27**, 13790.
- 141 K. Sugiyasu, N. Fujita and S. Shinkai, *Angew. Chem., Int. Ed.*, 2004, **43**, 1229.
- 142 H. Wang, X. Li, F. Fang and Y. Yang, *Dalton Trans.*, 2010, **39**, 7294.
- 143 M. J. Clemente, R. M. Tejedor, P. Romero, J. Fitremann and L. Oriol, *RSC Adv.*, 2012, **2**, 11419.
- 144 N. S. S. Kumar, S. Varghese, G. Narayan and S. Das, *Angew. Chem., Int. Ed.*, 2006, **45**, 6317.
- 145 D. G. Whitten, *Acc. Chem. Res.*, 1993, **26**, 502.
- 146 S. Wang, W. Shen, Y. Feng and H. Tian, *Chem. Commun.*, 2006, 1497.
- 147 L. Brunsveld, A. P. H. J. Schenning, M. A. C. Broeren, H. M. Janssen, J. A. J. M. Vekemans and E. W. Meijer, *Chem. Lett.*, 2000, 292.
- 148 A. Brizard, R. Oda and I. Huc, *Top. Curr. Chem.*, 2005, **256**, 167.
- 149 P. Jonkheijm, P. van der Schoot, A. P. H. J. Schenning and E. W. Meijer, *Science*, 2006, **313**, 80.
- 150 M. M. J. Smulders, A. P. H. J. Schenning and E. W. Meijer, *J. Am. Chem. Soc.*, 2008, **130**, 606.
- 151 T. Taniguchi and T. Usuki, *Supramolecular Chemistry: From Molecules to Nanomaterials*, Wiley-VCH, 2012.
- 152 D. K. Smith, *Chem. Soc. Rev.*, 2009, **38**, 684.
- 153 F. Allix, P. Curcio, Q. N. Pham, G. Pickaert and B. J. Grégoire, *Langmuir*, 2010, **26**, 16818.
- 154 M. J. Clemente, J. Fitremann, M. Mauzac, J. L. Serrano and L. Oriol, *Langmuir*, 2011, **27**, 15236.
- 155 Y. He, Z. Bian, C. Kang and L. Gao, *Chem. Commun.*, 2010, **46**, 5695.
- 156 M. Suzuki and K. Hanabusa, *Chem. Soc. Rev.*, 2009, **38**, 967.
- 157 C.-C. Tsai, W.-T. Chuang, Y.-F. Tsai, J.-T. Li, Y.-F. Wu and C.-C. Liao, *J. Mater. Chem. B*, 2013, **1**, 819.
- 158 X. Wang, P. Duan and M. Liu, *Chem. Commun.*, 2012, **48**, 7501.
- 159 Y. Li and M. Liu, *Chem. Commun.*, 2008, 5571.
- 160 J. E. Goldberger, E. J. Berns, R. Bitton, C. J. Newcomb and S. I. Stupp, *Angew. Chem., Int. Ed.*, 2011, **50**, 6292.
- 161 F. Rodríguez-Llansola, J. F. Miravet and B. Escuder, *Chem. Commun.*, 2009, 209.
- 162 Z.-T. Li and X. Zhao, *Supramolecular Chemistry: From Molecules to Nanomaterials*, Wiley-VCH, 2012.
- 163 S. Nandi, H.-J. Altenbach, B. Jakob, K. Lange, R. Ihizane, M. P. Schneider, Ü. Gün and A. Mayer, *Org. Lett.*, 2012, **14**, 3826.
- 164 S. Bhattacharya, A. Srivastava and A. Pal, *Angew. Chem., Int. Ed.*, 2006, **45**, 2934.
- 165 P. Byrne, G. O. Lloyd, L. Applegarth, K. M. Anderson, N. Clarke and J. W. Steed, *New J. Chem.*, 2010, **34**, 2261.
- 166 J.-S. Shen, G.-J. Mao, Y.-H. Zhou, Y.-B. Jiang and H.-W. Zhang, *Dalton Trans.*, 2010, **39**, 7054.
- 167 D. Das, T. Kar and P. K. Das, *Soft Matter*, 2012, **8**, 2348.
- 168 G. Pasparakis and M. Vamvakaki, *Polym. Chem.*, 2011, **2**, 1234.
- 169 E. Krieg, E. Shirman, H. Weissman, E. Shimoni, S. G. Wolf, I. Pinkas and B. Rybtchinski, *J. Am. Chem. Soc.*, 2009, **131**, 14365.
- 170 G. Bühler, M. C. Feiters, R. J. M. Nolte and K. H. Dötz, *Angew. Chem., Int. Ed.*, 2003, **42**, 2494.
- 171 S. P. Patil, H. S. Jeong and B. H. Kim, *Chem. Commun.*, 2012, **48**, 8901.
- 172 A. Brizard, M. Stuart, K. Bommel, A. Friggeri, M. Jong and J. Esch, *Angew. Chem., Int. Ed.*, 2008, **47**, 2063.
- 173 S. Mukhopadhyay, U. Maitra, G. Krishnamoorthy, J. Schmidt and Y. Talmon, *J. Am. Chem. Soc.*, 2004, **126**, 15905.
- 174 S. Yao, U. Beginn, T. Gress, M. Lysetska and F. Würthner, *J. Am. Chem. Soc.*, 2004, **126**, 8336.
- 175 R. W. Briehl, *Nature*, 1980, **288**, 622.
- 176 P. Mukhopadhyay, N. Fujita, A. Takada, T. Kishida, M. Shirakawa and S. Shinkai, *Angew. Chem., Int. Ed.*, 2010, **49**, 6338.
- 177 Z. M. Yang, H. W. Gu, Y. Zhang, L. Wang and B. Xu, *Chem. Commun.*, 2004, 208.
- 178 M. M. Smith and D. K. Smith, *Soft Matter*, 2011, **7**, 4856.
- 179 Y. Wang, L. Tang and J. Yu, *Cryst. Growth Des.*, 2008, **8**, 884.
- 180 S. S. Sheiko and M. Möller, *Chem. Rev.*, 2001, **101**, 4099.
- 181 Z. Qi, P. M. Molina, W. Jiang, Q. Wang, K. Nowosinski, A. Schulz, M. Grdzielski and C. A. Schalley, *Chem. Sci.*, 2012, **3**, 2073.
- 182 X. Zhang and C. Wang, *Chem. Soc. Rev.*, 2011, **40**, 94.
- 183 F. Biedermann, U. Rauwald, J. M. Zayed and O. A. Scherman, *Chem. Sci.*, 2011, **2**, 279.
- 184 Y. J. Jeon, P. K. Bharadwaj, S. W. Choi, J. W. Lee and K. Kim, *Angew. Chem., Int. Ed.*, 2002, **41**, 4474.
- 185 K. V. Rao, K. Jayaramulu, T. K. Maji and S. J. George, *Angew. Chem., Int. Ed.*, 2010, **49**, 4218.

- 186 J. B. Pawley, *Handbook of Biological Confocal Microscopy*, Springer, Berlin, 2006.
- 187 A. R. Hirst and D. K. Smith, *Chem.–Eur. J.*, 2005, **11**, 5496.
- 188 V. A. Mallia, P. Terech and R. G. Weiss, *J. Phys. Chem. B*, 2011, **115**, 12401.
- 189 W. Weng, Z. Li, A. M. Jamieson and S. J. Rowan, *Macromolecules*, 2009, **42**, 236.
- 190 W. Weng, J. B. Beck, A. M. Jamieson and S. J. Rowan, *J. Am. Chem. Soc.*, 2006, **128**, 11663.
- 191 W. Brown, *Dynamic Light Scattering: The Method and Some Applications*, Oxford University Press, 1993.
- 192 X. Liao, G. Chen, X. Liu, W. Chen, F. Chen and M. Jiang, *Angew. Chem., Int. Ed.*, 2010, **49**, 4409.
- 193 F. P. Schmidtchen, *Supramolecular Chemistry: From Molecules to Nanomaterials*, Wiley-VCH, 2012.
- 194 K. Kim, N. Selvapalam, Y. H. Ko, K. M. Park, D. Kim and J. Kim, *Chem. Soc. Rev.*, 2007, **36**, 267.
- 195 E. A. Appel, F. Biedermann, U. Rauwald, S. T. Jones, J. M. Zayed and O. A. Scherman, *J. Am. Chem. Soc.*, 2010, **132**, 14251.
- 196 B. Wunderlich, *Thermal Analysis*, Academic Press, New York, 1990.
- 197 Y. Wu, Y. Hirai, Y. Tsunobuchi, H. Tokoro, H. Eimura, M. Yoshio, S. Ohkoshi and T. Kato, *Chem. Sci.*, 2012, **3**, 3007.
- 198 C. Gong and H. W. Gibson, *J. Am. Chem. Soc.*, 1997, **119**, 5862.
- 199 H. Basit, A. Pal, S. Sen and S. Bhattacharya, *Chem.–Eur. J.*, 2008, **14**, 6534.
- 200 X. Cai, K. Liu, J. Yan, H. Zhang, X. Hou, Z. Liu and Y. Fang, *Soft Matter*, 2012, **8**, 3756.
- 201 W. C. Yount, D. M. Loveless and S. L. Craig, *Angew. Chem., Int. Ed.*, 2005, **44**, 2746.
- 202 S. K. Samanta, K. S. Subrahmanyam, S. Bhattacharya and C. N. R. Rao, *Chem.–Eur. J.*, 2012, **18**, 2890.
- 203 J. Yuan, X. Fang, L. Zhang, G. Hong, Y. Lin, Q. Zheng, Y. Xu, Y. Ruan, W. Weng, H. Xia and G. Chen, *J. Mater. Chem.*, 2012, **22**, 11515.
- 204 P. Sahoo, R. Sankolli, H.-Y. Lee, S. R. Raghavan and P. Dastidar, *Chem.–Eur. J.*, 2012, **18**, 8057.
- 205 X. Li, J. Li, Y. Gao, Y. Kuang, J. Shi and B. Xu, *J. Am. Chem. Soc.*, 2010, **132**, 17707.
- 206 F. Huang, D. S. Nagvekar, C. Slebodnick and H. W. Gibson, *J. Am. Chem. Soc.*, 2005, **127**, 484.
- 207 A. Dawn, T. Shiraki, H. Ichikawa, A. Takada, Y. Takahashi, Y. Tsuchiya, L. T. N. Lien and S. Shinkai, *J. Am. Chem. Soc.*, 2012, **134**, 2161.
- 208 K. Tiefenbacher, H. Dube, D. Ajami and J. Rebek, *Chem. Commun.*, 2011, **47**, 7341.
- 209 D. D. Díaz, D. Kühbeck and R. J. Koopmans, *Chem. Soc. Rev.*, 2011, **40**, 427.
- 210 M. Park, D. Jang, S. Y. Kim and J.-I. Hong, *New J. Chem.*, 2012, **36**, 1145.
- 211 E. Cheng, Y. Xing, P. Chen, Y. Yang, Y. Sun, D. Zhou, L. Xu, Q. Fan and D. Liu, *Angew. Chem., Int. Ed.*, 2009, **48**, 7660.
- 212 Q. Chen, Y. Lv, D. Zhang, G. Zhang, C. Liu and D. Zhu, *Langmuir*, 2010, **26**, 3165.
- 213 M.-O. M. Piepenbrock, G. O. Lloyd, N. Clarke and J. W. Steed, *Chem. Rev.*, 2010, **110**, 1960.
- 214 M. Zhang, D. Xu, X. Yan, J. Chen, S. Dong, B. Zheng and F. Huang, *Angew. Chem., Int. Ed.*, 2012, **51**, 7011.
- 215 Q. Wang, J. L. Mynar, M. Yoshida, E. Lee, M. Lee, K. Okuro, K. Kinbara and T. Aida, *Nature*, 2010, **463**, 339.
- 216 M. D. Hager, P. Greil, C. Leyens, S. D. Zwaag and U. S. Schubert, *Adv. Mater.*, 2010, **22**, 5424.
- 217 S. Burattini, B. W. Greenland, D. Chappell, H. M. Colquhoun and W. Hayes, *Chem. Soc. Rev.*, 2010, **39**, 1973.
- 218 B. Yang, Y. Zhang, X. Zhang, L. Tao, S. Li and Y. Wei, *Polym. Chem.*, 2012, **3**, 3235.
- 219 N. Park, S. H. Um, H. Funabashi, J. Xu and D. Luo, *Nat. Mater.*, 2009, **8**, 432.
- 220 C. T. S. W. P. Foo, J. S. Lee, W. Mulyasmita, A. Parisi-Amon and S. C. Heilshorn, *Proc. Natl. Acad. Sci. U. S. A.*, 2009, **106**, 22067.
- 221 H. D. Lu, M. B. Charati, I. L. Kim and J. A. Burdick, *Biomaterials*, 2012, **33**, 2145.
- 222 Y. Zhang, B. Yang, X. Zhang, L. Xu, L. Tao, S. Li and Y. Wei, *Chem. Commun.*, 2012, **48**, 9305.
- 223 Y. Liu, Y. Yu, J. Gao, Z. Wang and X. Zhang, *Angew. Chem., Int. Ed.*, 2010, **49**, 6576.
- 224 Y. Liu, Z. Wang and X. Zhang, *Chem. Soc. Rev.*, 2012, **41**, 5922.
- 225 S. Srinivasan, S. S. Babu, V. K. Praveen and A. Ajayaghosh, *Angew. Chem., Int. Ed.*, 2008, **47**, 5746.
- 226 J. K.-H. Hui, Z. Yu and M. J. MacLachlan, *Angew. Chem., Int. Ed.*, 2007, **46**, 7980.
- 227 J. Zhang, X.-D. Xu, L.-J. Chen, Q. Luo, N.-W. Wu, D.-X. Wang, X.-L. Zhao and H.-B. Yang, *Organometallics*, 2011, **30**, 4032.
- 228 L.-J. Chen, J. Zhang, J. He, X.-D. Xu, N.-W. Wu, D.-X. Wang, Z. Abliz and H.-B. Yang, *Organometallics*, 2011, **30**, 5590.
- 229 X.-D. Xu, J. Zhang, X. Yu, L.-J. Chen, D.-X. Wang, T. Yi, F. Li and H.-B. Yang, *Chem.–Eur. J.*, 2012, **18**, 16000.
- 230 O. Kretschmann, S. W. Choi, M. Miyauchi, I. Tomatsu, A. Harada and H. Ritter, *Angew. Chem., Int. Ed.*, 2006, **45**, 4361.
- 231 W. Deng and D. H. Thompson, *Soft Matter*, 2010, **6**, 1884.
- 232 S. Kiyonaka, K. Sugiyasu, S. Shinkai and I. Hamachi, *J. Am. Chem. Soc.*, 2002, **124**, 10954.
- 233 S.-L. Zhou, S. Matsumoto, H.-D. Tian, H. Yamane, A. Ojida, S. Kiyonaka and I. Hamachi, *Chem.–Eur. J.*, 2005, **11**, 1130.
- 234 Q. Chen, Y. Feng, D. Zhang, G. Zhang, Q. Fan, S. Sun and D. Zhu, *Adv. Funct. Mater.*, 2010, **20**, 36.